AGU PUBLICATIONS

Water Resources Research

RESEARCH ARTICLE
10.1002/2017WR021718

Lateral, Vertical, and Longitudinal Source Area Connectivity Drive Runoff and Carbon Export Across Watershed Scales

Margaret A. Zimmer[1,2] and Brian L. McGlynn[1]

[1]Division of Earth and Ocean Sciences, Duke University, Durham, NC, USA, [2]Now at Earth and Planetary Sciences Department, University of California, Santa Cruz, Santa Cruz, CA, USA

Key Points:
- Dynamic runoff source areas expanded and contracted laterally, longitudinally, and vertically in watersheds
- Landscape-specific variations in three-dimensional source area connectivity drove differences in runoff regimes across watershed scales
- Temporal variability of in-stream DOC export was driven by frequent event-based flushing and annual replenishment of DOC in shallow soil zones

Correspondence to:
M. A. Zimmer,
margaret.zimmer@ucsc.edu

Citation:
Zimmer, M. A., & McGlynn, B. L. (2018). Lateral, vertical, and longitudinal source area connectivity drive runoff and carbon export across watershed scales. *Water Resources Research*, *54*. https://doi.org/10.1002/2017WR021718

Received 16 AUG 2017
Accepted 1 FEB 2018
Accepted article online 16 FEB 2018

Abstract Watersheds are three-dimensional hydrologic systems where the longitudinal expansion/contraction of stream networks, vertical connection/disconnection between shallow and deep groundwater systems, and lateral connectivity of these water sources to streams mediate runoff production and nutrient export. The connectivity of runoff source areas during both baseflow and stormflow conditions and their combined influence on biogeochemical fluxes remain poorly understood. Here we focused on a set of 3.3 and 48.4 ha nested watersheds (North Carolina, USA). These watersheds comprise ephemeral and intermittent runoff-producing headwaters and perennial runoff-producing lowlands. Within these landscape elements, we characterized the timing and magnitude of precipitation, runoff, and runoff-generating flow paths. The active surface drainage network (ASDN) reflected connectivity to, and contributions from, source areas that differed under baseflow and stormflow conditions. The baseflow-associated ASDN expanded and contracted seasonally, driven by the rise and fall of the seasonal water table. Superimposed on this were event-activated source area contributions driven by connectivity to surficial and shallow subsurface flow paths. Frequently activated shallow flow paths also caused increased in-stream dissolved organic carbon (DOC) concentrations with increases in runoff across both watershed scales. The spread and variability within this DOC-runoff relationship was driven by a seasonal depletion of DOC from continual shallow subsurface flow path activation and subsequent replenishment from autumn litterfall. Our findings suggest that hydrobiogeochemical signals at larger watershed outlets can be driven by the expansion, contraction, and connection of lateral, longitudinal, and vertical source areas with distinct runoff generation processes.

1. Introduction

Watershed runoff source areas expand and contract due to the complex feedback between climatic forcings, antecedent storage conditions, and internal catchment processes that vary spatially across landscapes, as well as vertically with depth. The dominant dimensional variation in source areas has traditionally been expressed as changes in the lateral hydrologic connectivity (i.e., variable source area; Hewlett & Hibbert, 1967), which is often shown to be driven by surface runoff or the rise and fall of a water table across hillslopes adjacent to the stream (Bishop et al., 1993; Jencso et al., 2009; McGlynn & McDonnell, 2003b; Nippgen et al., 2015). The longitudinal expansion of river networks (Godsey & Kirchner, 2014; Phillips et al., 2011), as well as the vertical partitioning of shallow and deep groundwater systems (Tague et al., 2008; Zimmer & McGlynn, 2017b), are important additional source area dimensions that are not as well characterized or understood. The hydrologic connectivity of these source areas to the stream is highly variable laterally, longitudinally, and vertically in space, as well as through time (Ward, 1989), but few studies have taken a holistic approach toward understanding how these three-dimensional source areas contribute to runoff (Covino, 2017). For the purposes of this study, we define lateral, longitudinal, and vertical source area connectivity in Table 1. Furthermore, while the spatial partitioning and temporal behavior of these three-dimensional flow systems are poorly understood, their characteristics strongly affect the fluxes and processing of solutes and materials from the terrestrial environment to, and through, the aquatic system.

Streams are often viewed as a surficial expression of the subsurface aquifer system (Winter et al., 1998). Based on this concept, spatial assessments of flow in the stream network have been used to provide insight into the extent of water storage and availability in the subsurface (Godsey & Kirchner, 2014; Phillips et al., 2011). Although researchers have been investigating the mechanisms of stream network expansion and contraction for decades (e.g., Blyth & Rodda, 1973; Day, 1978), how network expansion/contraction

Table 1
Definitions for the Three-Dimensional Directions of Source Area Connectivity Investigated in This Study

Source area connectivity direction	Definition used in this study
Longitudinal	Longitudinal expansion of surface flow in drainage networks
Lateral	a. Surface and shallow subsurface lateral source area activation (e.g., shallow groundwater, floodplain inundation, wetland fill and spill)
	b. Deep lateral source area activation (e.g., deep groundwater)
Vertical	Saturated continuity between shallow and deep subsurface runoff sources

influences downstream dynamics remains poorly understood. One major hurdle in understanding when and where runoff will occur in a stream network is the variability in the spatial distribution of water storage across catchments (Bracken et al., 2013; Jencso et al., 2009; McNamara et al., 2011; Nippgen et al., 2015), which can result in complex runoff responses to precipitation inputs (Detty & McGuire, 2010; Zehe et al., 2005). Different runoff generation processes also exhibit different thresholds of activation (Allan & Roulet, 1994; Dunne, 1978; McNamara et al., 2005; Montgomery & Dietrich, 1994; Spence, 2007), which vary depending on antecedent conditions, climatic forcings, or geomorphology. As a result, conceptual models that explain surface drainage network expansion and contraction are still debated (Biswal & Marani, 2010; Godsey & Kirchner, 2014; Shaw, 2016; Whiting & Godsey, 2016).

Understanding the timing, magnitude, and origin of flow paths that drive runoff responses to water inputs is also critical for deciphering differences in biogeochemical dynamics across catchments. Typically, dissolved organic carbon (DOC) concentrations decrease and DOC variability dampens with increasing watershed size (Creed et al., 2015; Gannon et al., 2015; Temnerud & Bishop, 2005; Wolock et al., 1997), due to processes such as in-stream uptake, aggregation or changes in hydrological pathways, or adsorption to mineral surfaces (Creed et al., 2015; Kalbitz et al., 2000). The extent and location of landscape elements also strongly affect DOC export (e.g., Ågren et al., 2007; Laudon et al., 2011; McGlynn et al., 2004; Pacific et al., 2010). For instance, Inamdar et al. (2008) compared nitrogen and carbon export across catchments of different sizes and showed the importance of riparian zones and wetlands as DOC sources across scales. However, few studies have linked the lateral hydrologic connectivity of landscape elements with the longitudinal connectivity of surface drainage networks across watershed scales to better understand hydrologic and biogeochemical fluxes.

Geomorphically mature Piedmont landscapes physically connect mountain fronts to coastal plains. Within relatively low relief Piedmont landscapes, highly dissected headwater systems grade into valley bottoms. In arid and semiarid environments, these Piedmont regions have been linked to substantial groundwater recharge (Covino & McGlynn, 2007; Wilson & Guan, 2004). Humid regions are typically viewed as energy-limited systems (Budyko, 1974), with stream networks that have a net gain of groundwater (Winter et al., 1998). Recent work within humid Piedmont headwaters in North Carolina, USA (the location of this study; Table 2) has shown that nonperennial streams can contribute to groundwater recharge on an annual basis (Zimmer & McGlynn, 2017a) and that bidirectional hydraulic head gradients between the steam and local groundwater exist on a seasonal and event basis (Zimmer & McGlynn, 2017c). Outside the North Carolina Piedmont region, other studies have shown reversal of hydraulic gradients surrounding streams in low relief landscapes (Heeren et al., 2011, 2014; Vidon & Hill, 2004). It is not clear how the hydrology in low relief headwaters, specifically in the North Carolina Piedmont, which are often dominated by ephemeral and intermittent streams, influences the hydrology and biogeochemistry of their downstream perennial stream systems.

Here we examined the seasonality of landscape connectivity in lateral and longitudinal dimensions with foci on the roles of deep and shallow groundwater (vertically partitioned source areas) for dynamic runoff generation and DOC export in both ephemeral-to-intermittent headwater catchments and their downstream perennial waterways. To do this, we used field-collected hydrological and biogeochemical data from a 48.4 ha ephemeral-to-perennial drainage basin in the humid Piedmont region of North Carolina, USA. We investigated runoff and hydrochemical dynamics across two nested watersheds using in-stream and vertically distributed water table observations across landscape elements, active surface drainage network

Table 2
Description of Dominating Stream-Groundwater Interactions and Runoff Generation Mechanisms in Headwaters Within Catchment Storage States Based on Results From Zimmer and McGlynn (2017b)

		High catchment storage intermittent runoff regime	Low catchment storage ephemeral runoff regime
Seasonal time period; evapotranspirative demands		Winter and spring; low	Summer and fall; high
Directional gradient between deep seasonal water table and stream		Gaining stream system	Losing stream system
Dominant runoff flow paths to stream	Shallow flow paths	Saturated shallow flow paths activated based on rise of the seasonal water table into shallow soil horizons	Shallow, perched, transient water table activated by saturated perching on impeding soil horizons
	Deep flow paths	Seasonal water table rise based on accumulation of percolating water from low evapotranspirative demands	Depth of seasonal water table below stream (i.e., not contributing to runoff during this period)

Note. Catchment storage is driven by evapotranspirative demands as monthly precipitation is evenly distributed across the year.

(ASDN) expansion and contraction mapping, and catchment biogeochemistry to address the following questions:

1. What internal catchment processes drive the activation and connectivity of lateral, longitudinal, and vertical source area contributions to runoff?
2. How do these internal catchment processes and three-dimensional source area dynamics differ across watershed scales?
3. How does three-dimensional connectivity across the geomorphic drainage network impact biogeochemical dynamics observed at the watershed outlet?

2. Methods

2.1. Study Site

We conducted this study in a 48.4 ha ephemeral-to-perennial drainage basin located in the Duke Forest Research Watershed in North Carolina, USA (Figure 1). Ephemeral runoff is defined here as stormflow-activated runoff in otherwise dry channels. Intermittent runoff is defined here as seasonal runoff (>3 months of flow during the year) in otherwise dry channels. Perennial runoff is defined here as relatively (>90% of the time) permanent runoff in channels. Duke Forest has a humid subtropical climate with negligible seasonality in monthly precipitation and is almost entirely rain dominated with a long growing season that spans from April to October (Figure 2a). Approximately 1,376 mm of precipitation fell in the 2016 water year (1 October 2015 to 30 September 2016), which was slightly above normal (20% greater than mean precipitation over past 15 years; 8% greater than mean plus standard deviation over the past 15 years; NOAA, 2017). The mean annual temperature for Duke Forest is 15.5°C and mean annual evapotranspiration is 720 mm (Novick et al., 2015). All uses of the terminology "storage" or "storage state" refer to the relative wetness of the watershed (Figure 2a). High storage refers to periods when shallow soil moisture is high due to low evapotranspirative demands (dormant season) and low storage refers to periods when soil moisture is low due to high evapotranspirative demands (growing season).

The study site is located within the Carolina Slate Terrane, which is comprised of fine-grained felsic, metamorphic rock. Ultisol soils of the silt loam Georgeville series are predominant in this region (Bradley & Gay, 2005). These soils contain an argillic Bt horizon (i.e., an impeding soil layer), which is characterized by an increase in clay content and subsequent decrease in saturated hydraulic conductivity with depth (Soil Survey Staff, 2016). The elevation of the study site ranges from 165 to 210 m above mean sea level (a.m.s.l). The study watershed comprises two dominant landscape elements, specifically upstream headwater catchments and downstream lowlands (Figure 1). The downstream lowland landscape element (hereinafter referred to as lowlands) is dominated by gentler slopes (slope: mean = 14°, standard deviation = 6.6°), floodplains, and shallow (1–2 m) soils. This portion of the landscape is dominated by perennial runoff. The

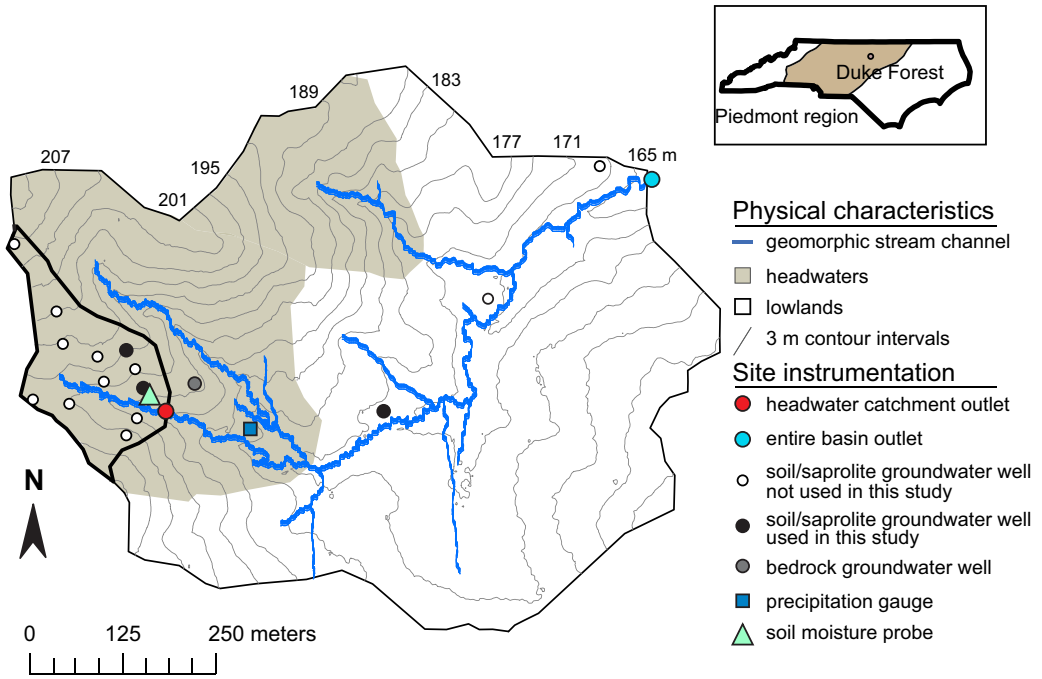

Figure 1. Geomorphic drainage network and instrumentation map for the 48.4 ha research basin. The boundary of the nested 3.3 ha zero-order headwater catchment is outlined as well. Top inset map indicates location of Duke Forest in North Carolina, USA, with shaded area indicating Piedmont physiographic region.

upper headwater portion of the watershed (hereinafter referred to as headwaters) comprises steeper slopes (mean = 16°, standard deviation = 4.9°) and deeper soils (1 to >9 m). This headwater system is characterized by flashy ephemeral and intermittent runoff.

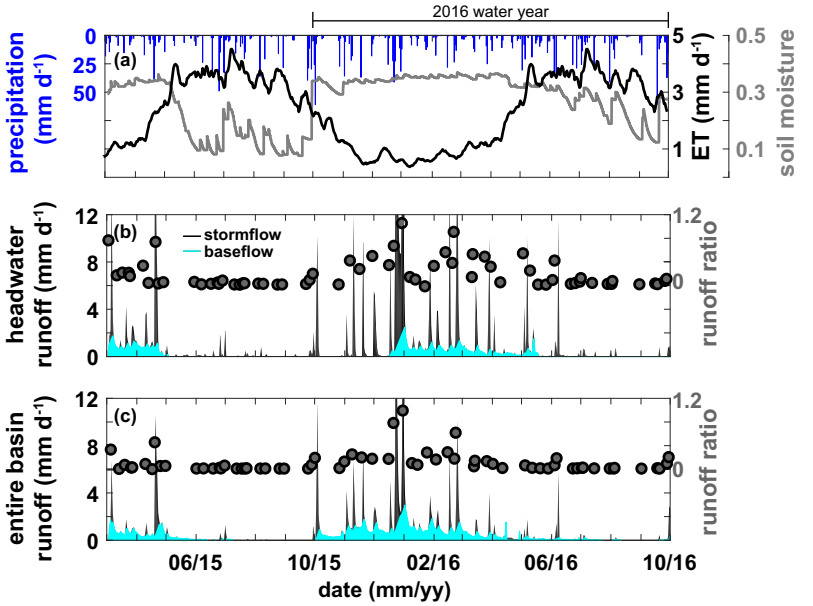

Figure 2. (a) Daily precipitation (blue bars), 3 day minimum volumetric water content (grey line) in the A horizon at lower hillslope in headwater catchment, and daily evapotranspiration (black line) as adapted from Novick et al. (2015). (b) Runoff ratios (grey circles) with time series of runoff separated into baseflow (light blue) and stormflow (black) components for the zeroth-order headwater catchment (3.3 ha). (c) Runoff ratios (grey circles) with time series of runoff separated into baseflow (light blue) and stormflow (black) components for the outlet of the first-order basin (48.4 ha). Data from Figures 2a and 2b subplots also shown in Zimmer and McGlynn (2017b).

Widespread agriculture dominated the landscape in the eighteenth through early twentieth centuries (Richter et al., 1999). The landscape is now dominated by forest that is approximately 80–100 years old (Oishi et al., 2008) and contains a mix of deciduous hardwoods, including oaks (*Quercus* spp.), hickories (*Carya* spp.), elms (*Ulmus* spp.), sweetgum (*Liquidambar styraciflua*), and tulip poplar (*Liriodendron tulipifera*). Within these forests are stands of mature natural and planted pine (predominately loblolly pine, *Pinus taeda*).

2.2. Hydrochemical Sensor Installations, Measurements, and Analyses

2.2.1. Hydrometric Installation and Measurements

We focused instrumentation and analysis on two spatial scales, specifically the entire 48.4 ha basin scale and, nested within this, a 3.3 ha headwater catchment scale (Figure 1 and Table 3). We utilized a suite of field data, including runoff, precipitation, and groundwater levels collected from 3 March 2015 through 30 September 2016. At the entire 48.4 ha basin outlet, we recorded 5 min stage data from a stilling well installed in-channel (Figure 1) using a capacitance water level recorder ($\pm$1 mm resolution; TruTrack Inc., New Zealand) and converted to discharge using a field-developed rating curve that spanned the range of observed flow conditions (10th to 88th flow percentiles). At the 3.3 ha headwater catchment outlet, we recorded 5 min stage data from a stilling well located within a 0.91 m (3 ft) H-flume (Figure 1) using a capacitance water level recorder and converted to discharge using a field-verified geometric relationship between water height in the flume and runoff (U.S. Department of Agriculture, 1972). We recorded precipitation inputs at 5 min intervals using a 0.1 mm increment tipping bucket (Campbell Scientific, USA) located in a small forest clearing approximately 200 m downstream of the headwater catchment outlet (Figure 1), within the 48.4 ha basin. Due to the minimal elevation change and small spatial extent of the 48.4 ha study site, precipitation inputs were treated as spatially uniform.

We monitored shallow and deep groundwater levels at 5 min intervals in 12 locations across the 3.3 ha headwater catchment and integrated (i.e., wells fully screened) groundwater levels at three locations across the lowlands (Figures 1 and 3) using a combination of capacitance water level recorders ($\pm$1 mm resolution; TruTrack Inc., New Zealand) and pressure transducers ($\pm$0.1 mm resolution; Solinst, CA, USA). For this study, we used a subset of characteristic wells. In the headwater catchment, wells were distributed across a range of landscape positions, including lower, mid and upper hillslope locations within convergent and planar hillslopes. Shallow wells were installed to the A/Bt and Bt/C horizon interfaces (Figure 3), which were locations of rapid decrease in saturated hydraulic conductivity (see Zimmer & McGlynn, 2017b for more details on soil characteristics and groundwater well installation). Deep groundwater wells were installed to hand-augered refusal depths, representative of the transitional zone between lower saprolite and the upper weathering front of the competent bedrock (Figure 3). Depths to refusal varied considerably across the study site. In the headwater catchment, the depth to the upper bedrock weathering front increased away from the stream, with shallow soil and saprolite in the lower hillslopes ($\sim$1 m) and deeper soil and saprolite in the upper hillslopes ($>$9 m). Downstream of the 3.3 ha headwater catchment, wells were installed approximately 1–1.5 m to hand-augered refusal depths in three lowland locations between 10 and 20 m from the stream channel (Figures 1 and 3). A bedrock groundwater well was installed to 25 m depth on a ridgeline just outside the headwater catchment. Depth to competent bedrock at this location was 3.6 m.

Table 3
Physical Landscape Attributes and 2016 Water Year Hydrologic Characteristics for the Headwater Catchment and the Entire Research Basin

	Headwater catchment	Entire basin
Watershed size (ha)	3.3	48.4 (62% lowlands, 28% headwaters)
Slope (°)	Mean = 16; standard deviation = 4.9	Mean = 14; standard deviation = 6.6
Annual runoff (mm)	544	397
Runoff ratio	0.39	0.29
Annual baseflow (mm)	93	167
Baseflow as fraction of total runoff	0.17	0.42
Annual groundwater recharge (mm)	112	261
Recharge as fraction of total runoff	0.08	0.19

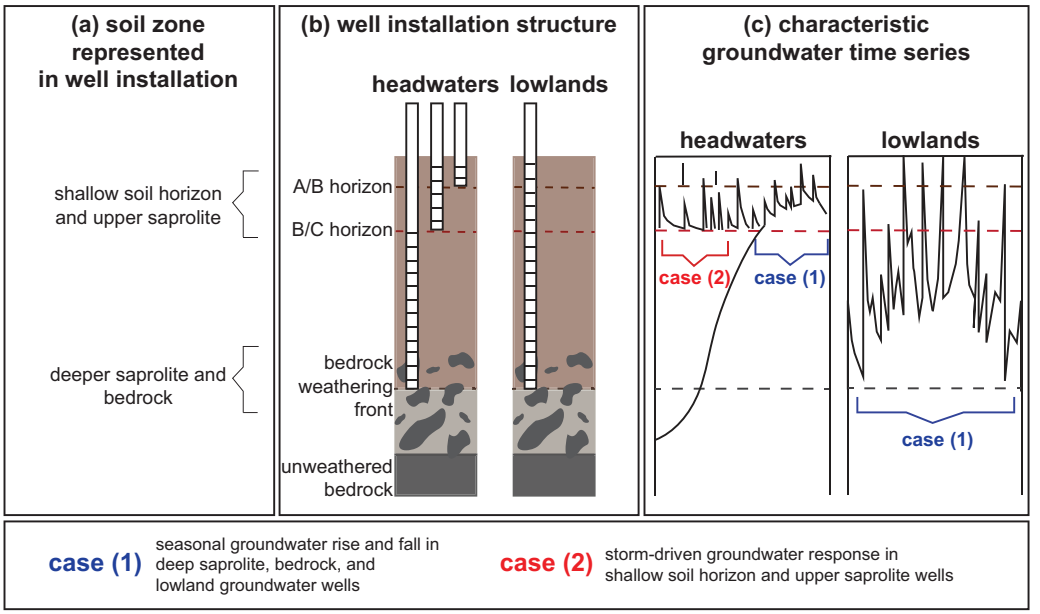

Figure 3. Groundwater installation scheme across landscape elements to capture two different groundwater flow regimes. (a) Groundwater level dynamics in different subsurface soil zones captured by different well installations and screening depths. (b) Well installation configurations varied by location. In the headwaters, multiple groundwater wells were installed together to monitor shallow and deep groundwater levels. In the lowlands, a singular well was installed to refusal. (c) Characteristic groundwater time series across landscape elements, as captured by well installation structures. The time series in this figure are not real data, are just for demonstrational purposes and portions of the figure are adapted from Zimmer and McGlynn (2017b). Case 1 represents a seasonal water table that rises and falls throughout the year. Case 2 represents perched groundwater flow responses that are activated in response to precipitation events.

Evapotranspiration was estimated from an 8 year data set (2001–2008) of 30 min data collected from an eddy covariance flux tower within a section of the Duke Forest located $<$6 km away, characterized by similar elevation ($\sim$163 m a.m.s.l.) and vegetation (pine and hardwood; Novick et al., 2015). Annual precipitation across the 8 year study varied by $\pm$200 mm, including two approximately 1 year long drought periods. During the study period, precipitation inputs were slightly higher (20% above average) and followed a typical precipitation year in 2015 ($<$1% different from average). To create a representative daily evapotranspiration time series for our study period given the 8 year historical data record, we averaged daily values from four consecutive nondrought years within the Novick et al. (2015) data set (Figure 2).

2.2.2. Hydrochemical Sensor Installation and Measurements

At the gauging stations of the headwater catchment and the entire basin (Figure 1), we installed in-stream specific conductance probes (Campbell Scientific, USA) and multiple water quality parameter sonde optical sensors (YSI EXO 2; California, USA). These optical sensors recorded water quality measurements at 5–15 min intervals. Integrated nylon brush wipers cleaned the optical lenses every 72 h and we manually cleaned the lenses weekly. We used calibration solution to test for instrument drift every 3–6 months and recalibrated the sensors if $>$10% difference from the calibration solution was measured, which occurred roughly every 6–9 months. For the purposes of this study, only the fluorescent dissolved organic matter (fDOM; defined as the fraction of colored DOM that fluoresces) time series, which is measured in quinine sulfate units (QSU; $\pm$0.01 ppb QSU resolution) from the EXO 2, is presented. We collected discrete grab samples of stream water biweekly and more frequently during select precipitation events to measure DOC concentrations in the laboratory. Samples were collected in HDPE bottles, filtered through 0.45 μm polyethersulfone (PES) filters (Whatman Puradisc 25 mm syringe filters and 46 mm vacuum filters) into opaque brown bottles, and acidified to a pH of 1–2 using 6 N HCl acid. Samples were refrigerated until analysis of total DOC concentrations on a Duke University Schimadzu total carbon analyzer (Shimadzu TOC-V CPH Total Organic Carbon Analyzer with ASI-V autosampler, Kyoto, Japan). We used the linear regression between DOC (mg/L) from the discrete grab samples and measured fDOM from the EXO 2 to derive a time series of DOC concentrations from the high-frequency fDOM time series at the headwater outlet ($n = 99$, $r^2 = 0.82$) and at the entire basin outlet ($n = 79$; $r^2 = 0.78$).

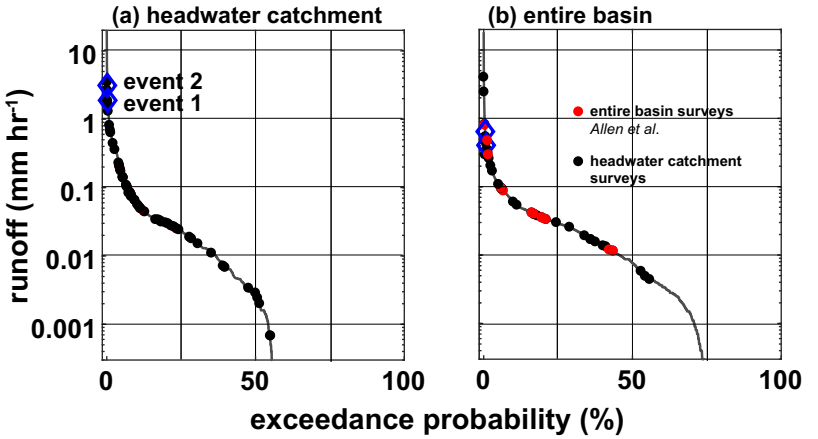

Figure 4. Exceedance probability curves for (a) headwater catchment outlet runoff and (b) entire basin outlet runoff across the entire study period, March 2015 to October 2016. Black circles represent runoff conditions during the ASDN surveys taken only within the headwater catchment. Red circles represent runoff conditions during the surveys taken across the entire basin (Allen et al., 2018). Blue open diamonds represent surveys taken during the two precipitation events highlighted in Results (section 3.2).

2.3. Landscape Element Delineation and Active Surface Drainage Network Length Surveys

The study site is comprised of headwaters and lowlands (Figure 1), which we delineated based on topographic slope breaks between planar, low relief lowland areas and steeper, more convex and concave headwaters. We paired this terrain analysis with direct and long-term observations of approximate locations of shifts from perennial to nonperennial runoff across the drainage network. We did this within the headwater catchment through 77 surveys of active surface drainage network (ASDN, i.e., active stream network) length across a broad range of flow conditions (Figure 4a; see Zimmer & McGlynn, 2017b for full details). Each survey consisted of walking the drainage network and recording presence or absence of flow every meter by averaging the degree of connectedness (0–10 scale) across every 10 m section. From each survey, the total ASDN length (km) was converted to ASDN density (km/km^2) by dividing stream length by the 3.3 ha (0.03 km^2) catchment area. From these 77 surveys, a nonlinear regression between ASDN density and runoff at the time of measurement was calculated ($r^2 = 0.79$; Figure 5a) and used to derive a time series of the ASDN density from the 5 min time series of runoff at the headwater outlet (Figure 5b). In a related study, Allen et al. (2018) measured the ASDN length across the entire 48.4 ha basin 12 times (red dots in Figure 4b). Similar to the headwater surveys, these network lengths were divided by the basin area to convert units to an ASDN density. A comparison between ASDN densities between the 3.3 ha headwater catchment and the entire 48.4 ha basin showed similar expansion dynamics across scales (Figures 5a and 5c). Given these similarities in ASDN densities, we used our ASDN surveys from the headwater catchment to fill in data gaps in the entire 48.4 ha basin ASDN surveys (black dots in Figure 4b) in order to create another nonlinear regression between ASDN density and runoff at the outlet for the entire 48.4 ha basin ($r^2 = 0.70$; Figure 5c). From this, we derived an additional ASDN density time series from the 5 min runoff time series at the entire basin outlet (Figure 5d).

2.4. Hydrological and Biogeochemical Calculations

2.4.1. Baseflow Separation of Watershed Outlet Hydrographs and Spatial Runoff Contributions to Drainage Network

During periods of the year when the channel was dry and runoff occurred only in direct response to precipitation inputs (i.e., ephemeral runoff), we categorized all runoff as stormflow derived (Figure 2). During periods with persistent runoff (i.e., intermittent or perennial), we conducted a hydrograph separation of baseflow and stormflow runoff components (Figure 2). The hydrograph separation method presented by Hewlett and Hibbert (1967) was adapted to separate baseflow from stormflow using a linear increase in baseflow contributions across 5 min interval time steps during precipitation events. We adjusted the Hewlett and Hibbert (1967) linear baseflow contribution increase to 0.00012 and 0.000036 mm/h for the 3.3 ha headwater catchment and the entire 48.4 ha basin, respectively, to account for the flashier nature of the headwater catchment. These different linear increases in baseflow contributions during events were used

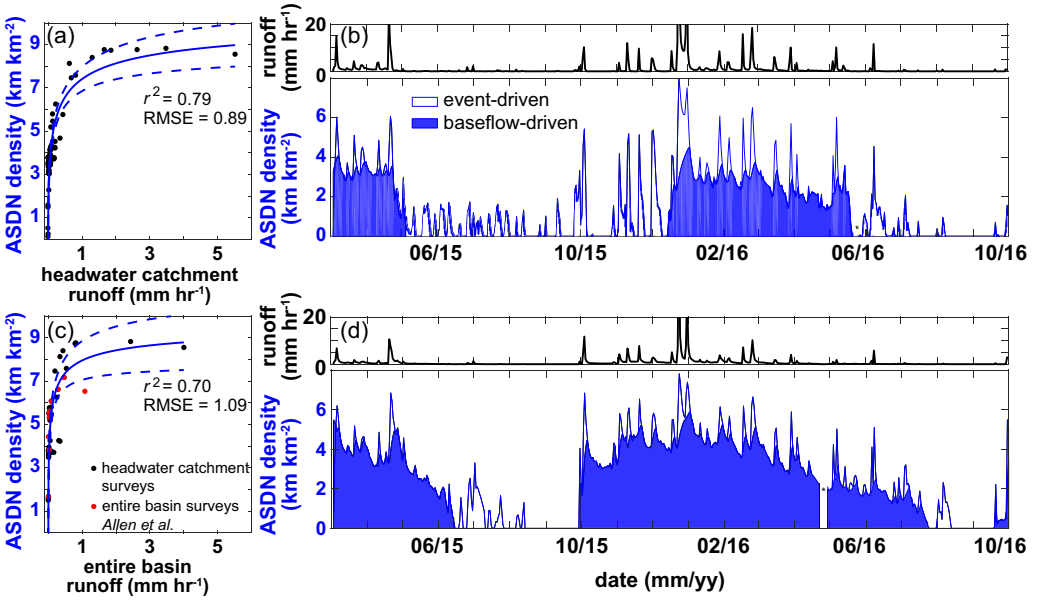

Figure 5. (a) Regression (blue line) with ±95% confidence intervals (dashed blue lines) fitted to relationship between ASDN density and runoff from surveys in headwater catchment. (b) (top) Runoff and (bottom) derived ASDN density time series from regression in Figure 5a. (c) Regression (blue line) with ±95% confidence intervals (dashed blue lines) for ASDN density versus runoff from surveys from entire watershed (red circles; Allen et al., 2018) and supplemented with runoff at the entire basin outlet during surveys from headwater catchment. (d) (top) Runoff and (bottom) derived ASDN density time series from regression in Figure 5c. Asterisk refers to missing data.

to obtain annual runoff ratios similar to those derived from a US Geological Survey baseflow index estimation report (Wolock, 2003). Runoff during interstorm periods was assumed to be comprised entirely of baseflow.

The ASDN expanded and contracted seasonally due to changes in baseflow contributions as well as temporarily during precipitation events due to stormflow contributions (Figure 5). In many landscapes, including the Piedmont region of North Carolina, USA, baseflow contributions are driven by deep subsurface flow paths and groundwater sources, while stormflow contributions are driven by surface and shallow subsurface flow paths (Winter et al., 1998; Zimmer & McGlynn, 2017b). To quantify the impact of these source dynamics on the expansion and contraction of the ASDN, we utilized the baseflow runoff time series (Figure 2) to derive the baseflow-associated ASDN (Figures 5b and 5d). We did this by applying the same relationship between ASDN density and runoff described in section 2.3 to the baseflow runoff time series. We classified the difference between the total ASDN and this baseflow-associated ASDN as the stormflow-driven ASDN (Figures 5b and 5d). This baseflow separation was done for both the 3.3 ha headwater catchment outlet and entire 48.4 ha basin outlet.

2.4.2. Event Runoff Ratios and Landscape Element Runoff Contributions to Stormflow

We calculated runoff ratios for 60 individual events across the study period by dividing total event stormflow by total event precipitation, where stormflow was calculated as total runoff minus the baseflow component. We calculated separate runoff ratios for both the entire 48.4 ha basin and the 3.3 ha headwater catchment. Events were defined by >8 mm precipitation separated by >24 h of no precipitation, in order to isolate individual stormflow hydrographs. The 8 mm precipitation threshold was chosen as it systematically produced enough stormflow responses to be discernable from instrument error. For these event criteria, runoff was always present at both watershed scales.

We performed single variable and stepwise multiple linear regressions between runoff ratios and potential explanatory variables (Table 4). While hydrologic relationships are often complex, we chose to assume linearity to help us seek and identify underlying relationships. We performed these analyses for runoff ratios from the headwater catchment, for the entire basin, and for the ratio of the headwater and entire basin runoff ratios (hereinafter referred to as the ratio of runoff ratios), which allowed for additional comparison of runoff behavior across scales. For the single variable linear regression analysis, we employed the fitlm

Table 4
r^2 and Root-Mean-Square Error (RMSE) for Linear Regressions Between Individual Explanatory Variables and Runoff Ratios for the Headwater Catchment and the Entire Basin, As Well As the Ratio of Runoff Ratios

Explanatory variable	Representative process/characteristic	Headwater runoff ratio r^2, RMSE (direction)	Entire basin runoff ratio r^2, RMSE (direction)	Ratio of headwater and entire basin runoff r^2, RMSE (direction)
Headwater total runoff	Event characteristic	0.72, 0.17 (+)[b]	0.71, 0.1 (+)[b]	0.02, 12.4 (–)
Entire basin total runoff	Event characteristic	0.7, 0.18 (+)[b]	0.76, 0.09 (+)[b]	0.03, 12.3 (–)
Precipitation total	Event characteristic	0.12, 0.31 (+)[b]	0.19, 0.17 (+)[b]	0.03, 12.3 (–)
Maximum hourly precipitation intensity	Event characteristic	0.02, 0.33 (–)	0.00, 0.19 (–)	0.00, 12.4 (+)
Daily evapotranspiration	Seasonality/storage state	0.33, 0.27 (–)[b]	0.29, 0.16 (–)[b]	0.12, 11.7 (+)[b]
Three day minimum antecedent shallow soil water content	Seasonality/storage state	0.23, 0.29 (+)[b]	0.18, 0.17 (+)[b]	0.22, 11 (–)[b]
Peak ASDN density	Event characteristic and seasonality/ storage state	0.43, 0.25 (+)[b]	0.47, 0.14 (+)[b]	0.23, 10.9 (–)
Peak deep groundwater level	Event characteristic and seasonality/ storage state	0.26, 0.28 (+)[b]	0.17, 0.17 (+)[b]	0.07, 12.1 (–)
Day within water year	Seasonality/storage state	0.25, 0.29 (–)[b]	0.23, 0.17 (–)[b]	0.06, 12.1 (+)
	Best stepwise multiple linear regression[a]	0.55[c] (precipitation total, peak ASDN density, peak deep groundwater level)	0.47[c] (peak ASDN density)	0.29[c] (peak ASDN density, antecedent shallow soil water content)

Note. Direction of fit in parentheses.
[a]Multiple linear regression from stepwise function used all explanatory variables except first two rows (total runoffs from headwater and entire basin) as they were highly correlated to one another. [b]Significant relationship with p-value <0.01. [c]r^2 value (variables included in best regression).

function in MATLAB (version 2016b) to derive r^2 and root-mean-squared error (RMSE) values between each variable and the runoff ratios. We defined $r^2 < 0.04$ as nonexistent relationships, $0.04 < r^2 < 0.3$ as weak relationships, $0.3 < r^2 < 0.5$ as moderate-strength relationships, $0.5 < r^2 < 0.8$ as strong relationships, and $0.8 < r^2$ as very strong relationships. For the multiple linear regression analysis, we employed stepwisefit function in MATLAB (entrance/exit tolerances set at 0.05/0.10 p-values) to derive r^2 and RMSE values of the best multiple linear combination of explanatory variables.

Although the delineated headwaters included portions of the study site outside the headwater catchment gauging station (Figure 1), a quantitative geospatial landscape analysis and qualitative observations of runoff regimes confirmed that the 3.3 ha headwater catchment is characteristic of the overall headwater landscape. Thus, we scaled the volumetric discharge from the 3.3 ha headwater catchment to the total headwater landscape area (18.7 ha) to calculate total discharge originating from headwaters. We subtracted this value from the discharge measured at the 48.4 ha basin outlet to derive the runoff losses and gains from the lowlands.

Similar to the headwater and lowland partitioning of runoff contributions described above, we calculated the DOC fluxes from the upstream headwaters and downstream lowlands. We scaled the time-integrated DOC flux (DOC concentration multiplied by discharge across each measurement interval) from the 3.3 ha headwater catchment to the total headwater landscape area (18.7 ha) to estimate the total DOC fluxes from headwaters. We subtracted this value from the time-integrated DOC flux from the 48.4 ha basin outlet to derive fluxes into and out of the lowlands.

3. Results

3.1. Runoff

Runoff was highly responsive to precipitation inputs, but flashiness appeared to decrease with spatial scale (Figure 2). In the 2016 water year, 544 mm of runoff at the 3.3 ha headwater catchment outlet and 397 mm of runoff at the entire 48.4 ha basin outlet were measured (Table 3). Baseflow comprised 17 and 42% of annual runoff at the headwater catchment and entire basin outlets, respectively (Table 3).

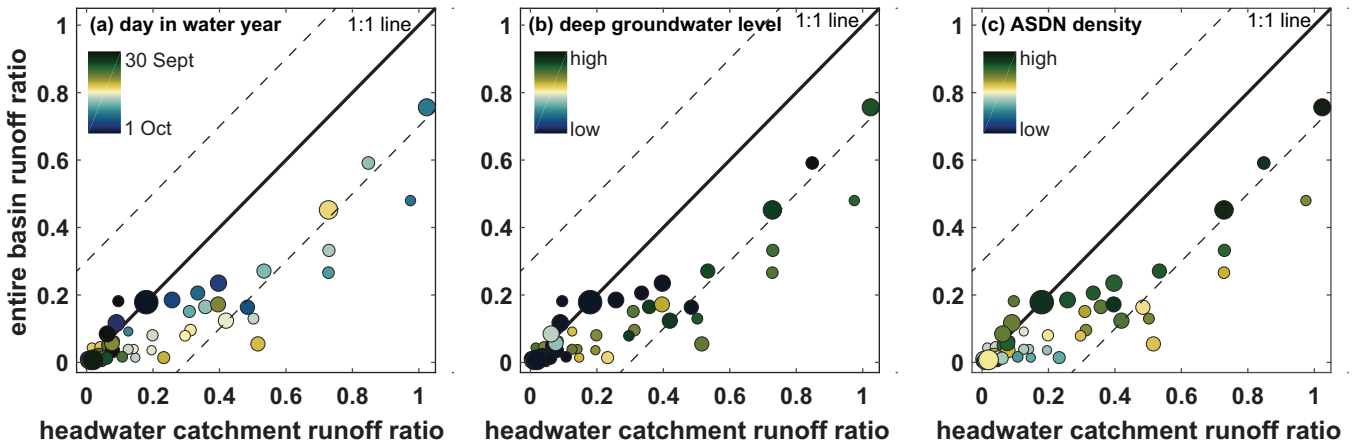

Figure 6. Runoff ratios from the outlet of entire basin versus runoff ratios from the headwater catchment outlet. Circle size is proportional to relative precipitation amount. Dashed lines parallel to 1:1 line are included to help guide the reader.

Runoff ratios for individual precipitation events varied seasonally (Figures 2 and 6). Generally, low runoff ratios occurred when evapotranspiration was high and groundwater levels and soil moisture were low (summer and fall months). Higher runoff ratios occurred when evapotranspiration was low and groundwater levels and soil moisture were high (winter and spring months). As shown in Figure 6, the headwater catchment and the entire basin had comparable runoff ratios at low values (0–0.1). As runoff ratios increased to between 0.1 and 0.5, the headwater catchment produced consistently more runoff than the entire basin. Above 0.5, there was a similar increase in runoff ratios for the two scales (Figure 6).

Results from the linear regression analysis (Table 4) indicated that runoff ratio variability in the headwater catchment was explained best by total event runoff ($r^2 = 0.72$), peak ASDN density ($r^2 = 0.43$) and daily evapotranspiration ($r^2 = 0.33$). In a stepwise multiple linear regression analysis that excluded total runoff values because they dominated the regression results, precipitation, groundwater level peak, and drainage density peak best explained runoff ratios for the headwater catchment ($r^2 = 0.55$). Runoff ratio variability at the entire basin scale was explained best by total event runoff at either watershed scale ($r^2 > 0.71$) or peak ASDN density ($r^2 = 0.47$). In the stepwise multiple linear regression for the entire basin, peak drainage density best explained runoff ratios ($r^2 = 0.47$). For the ratio of runoff ratios, drainage density ($r^2 = 0.23$) and 3 day minimum antecedent shallow soil moisture ($r^2 = 0.22$) were the most important descriptors of runoff behavior, though we still consider these weak relationships. Total event runoff appeared to have little influence on the ratio of runoff ratios ($r^2 = 0.03$). Peak ASDN density and antecedent shallow soil water content best explained the ratio of runoff ratios in a stepwise multiple linear regression ($r^2 = 0.29$).

Results from the subtraction of total headwater runoff from runoff at the entire basin outlet indicated strong seasonality in source area contributions from the lowlands (Figure 7). From fall through early spring, when evapotranspiration was low and storage was high, runoff from the lowlands dominated the 3 day mean runoff signal at the entire basin outlet (represented by positive blue areas in Figure 7c). During these periods, dominant runoff contributing areas differed for individual events, shifting from headwater-dominated source areas at the beginning of precipitation events toward lowland-dominated source areas later in the event (event dynamics represented with black line in Figure 7b). From late spring through early fall, when evapotranspiration was high and storage was low, runoff from the headwaters dominated the 1 h mean runoff at the entire basin outlet during precipitation events (event dynamics represented with black line in Figure 7b). Interstorm periods showed minimal runoff at either spatial scale during this period.

3.2. Active Surface Drainage Network

The ASDN density ranged from 0 to 8 km/km^2, depending on the seasonal catchment storage state and event-based precipitation and storage dynamics (Figure 5). On a seasonal basis, the ASDN expanded and contracted based on fluctuations in baseflow (Figures 5b and 5d). Superimposed on this, the ASDN expanded and contracted due to storm-driven contributions during precipitation events

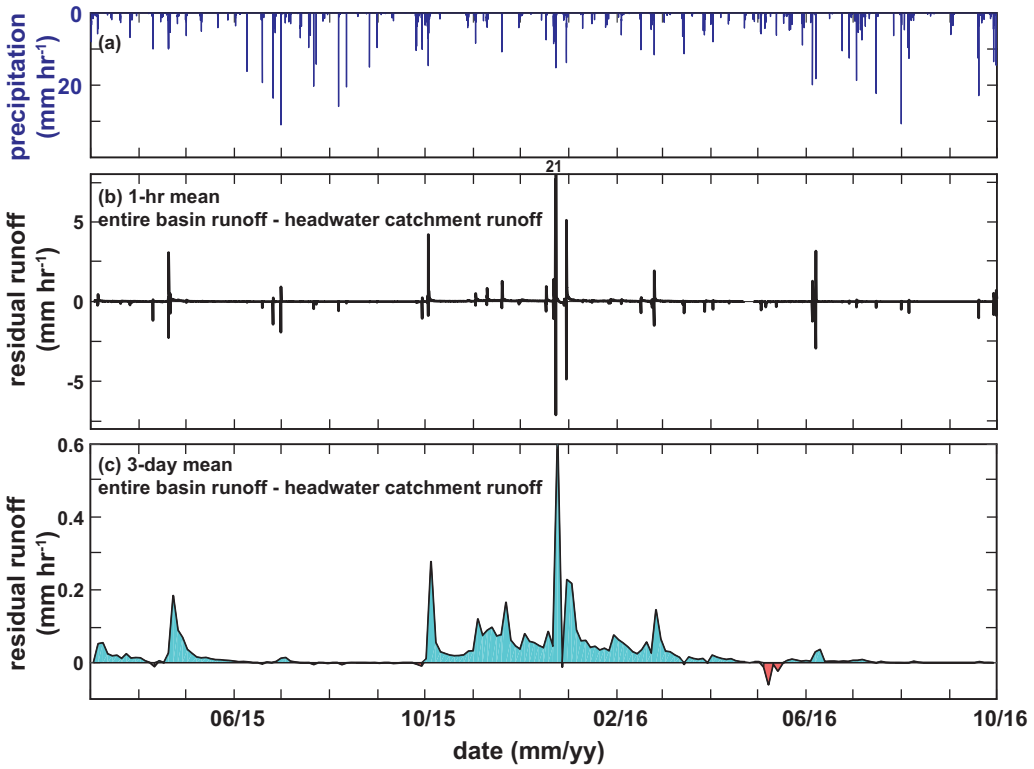

Figure 7. (a) Precipitation time series across the study period. (b) One hour mean time series of residual runoff as calculated by runoff from the entire basin subtracted by runoff from the headwaters. The small number represents a peak above 8 mm/h. (c) Three day mean time series of residual runoff as calculated by runoff from the entire basin minus the runoff from headwaters. Positive values in Figures 7b and 7c represent periods when entire basin runoff contributions are greater than headwater runoff contributions. Negative values represent periods when headwater runoff contributions are greater than entire basin runoff contributions.

(Figures 5b and 5d). These seasonal and event-based ASDN density dynamics affected the entire basin and headwater runoff ratios (Table 3 and Figure 6).

These two runoff regimes (i.e., baseflow-associated and event-driven) had different magnitudes and temporal characteristics at the headwater catchment and entire basin study scales. In the headwaters, the ASDN was driven solely by storm event-driven expansion and contraction during roughly two thirds of the study period (Figure 5b). During periods when baseflow did contribute to the ASDN (predominantly winter and spring periods), storm event-driven contributions still played a significant role in stream network dynamics. At the scale of the entire basin, the baseflow network length dominated much of the ASDN both in magnitude and frequency (Figure 5d). During short periods in the summer, when evapotranspiration was high and storage was low, ASDN across the entire basin was activated solely by storm event-driven runoff contributions (Figure 5d).

3.3. Shallow and Deep Groundwater Systems

Shallow and deep groundwater dynamics in the headwater catchment are described in detail in Zimmer and McGlynn (2017b) and summarized in relation to catchment storage and runoff dynamics in Table 2. Figure 8 presents the relationship between groundwater level and runoff for a subset of characteristic shallow and deep groundwater wells within the headwaters (Figures 8a and 8b) and the lowlands (Figures 8c and 8d).

In the headwaters, the presence of groundwater in shallow wells, from either a rise of the deeper groundwater or from activation of a shallow, perched water table, was necessary for runoff activation (Figure 8a). The deeper water table was not always necessary for runoff to occur in the headwaters (Figure 8b) as runoff was observed during both the presence and absence of deep groundwater. This deep groundwater system was highly dependent on season, and thus storage state, of the catchment (Figure 8b). The seasonal rise of

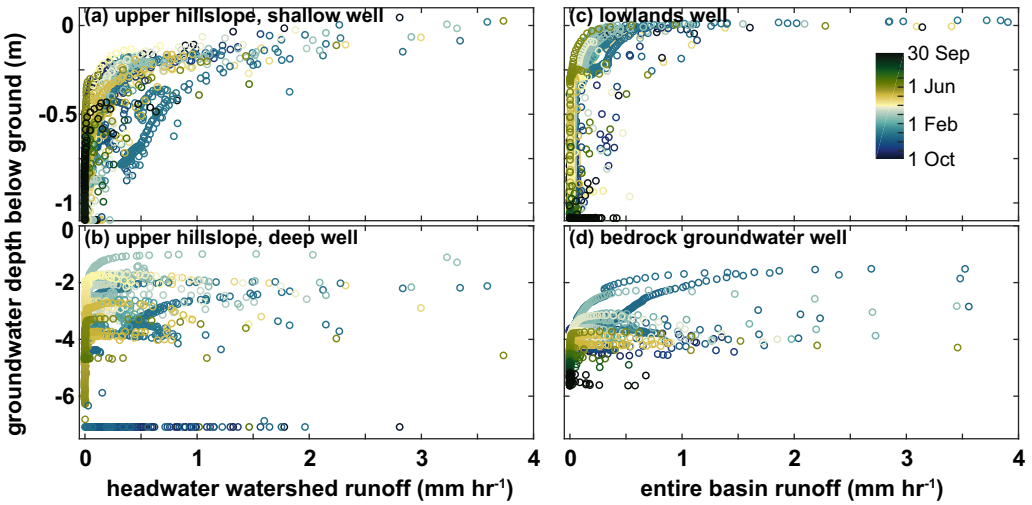

Figure 8. Groundwater depths below ground versus runoff at the two watershed scales. Color gradient represents time. Please note the differences in scales between the top and bottom subplots.

this deep system above the stream channel shifted groundwater gradients toward the channel (see Zimmer & McGlynn, 2017a for more information on groundwater-stream gradient shifts). This shifted the runoff regime of the headwater catchment from ephemeral (i.e., runoff activated in response to precipitation in an otherwise dry channel) to intermittent (persistent seasonal runoff; Table 2).

In the lowlands, groundwater levels were highly responsive to precipitation inputs, as suggested by their relationship with runoff (Figure 8c). While there was some scatter, there was generally a consistent and seasonally independent relationship (Figure 8c), similar to the shallow well dynamics seen in the headwaters (Figure 8a).

Deeper groundwater levels in the lowlands showed strong seasonality, which was consistent with deep groundwater measured in the bedrock well (Figures 8b and 8d). Bedrock groundwater levels were at a minimum in early fall when catchment storage was at its lowest and at a maximum in winter when catchment storage was at its highest. This steady seasonal rise was driven by a balance between seasonal shallow evapotranspirative demands and continuous percolation of precipitation inputs from individual events.

3.4. Stream Water Dissolved Organic Carbon Concentrations

Dissolved organic carbon (DOC) concentrations in stream water increased with increases in runoff and ASDN density across both watershed scales (Figure 9). This DOC concentration-runoff relationship has a logarithmic shape with maximum concentrations approaching 25 and 30 mg/L at the headwater catchment and the entire basin outlets, respectively (Figures 9a and 9c).

At the 3.3 ha headwater catchment outlet, in-stream DOC concentrations rose quickly from ~1 to 7.5 mg/L at low runoff (0–0.1 mm/h; Figure 9a). At intermediate runoff values (0.1–0.6 mm/h), there was strong seasonality in the steepness of the DOC concentration-runoff relationship. The increase in the rates of DOC concentration with runoff was highest during fall periods and lowest in late spring. At runoff above 0.6 mm/h, the rates of DOC concentration increase with runoff appeared to begin to flatten and maximum DOC concentrations were seasonally variable. High and low DOC concentrations occurred in fall through winter and spring through summer, respectively. Since the ASDN density was calculated as a function of runoff, seasonal patterns between DOC concentrations and ASDN density were similar to those between DOC concentrations and runoff, although the shapes of the overall relationships were different. At low ASDN densities, fall periods had higher DOC concentrations and early summer had lower DOC concentrations (Figure 9b). For ASDN densities above 2.5 km/km^2, a linear increase in DOC concentrations with runoff occurred, with lower concentrations in spring through summer and higher concentrations in fall through winter.

At the entire 48.4 ha basin outlet, DOC concentration dynamics showed similar responses to fluctuations in runoff to those seen at the 3.3 ha headwater catchment outlet (Figure 9). At the entire basin outlet, DOC

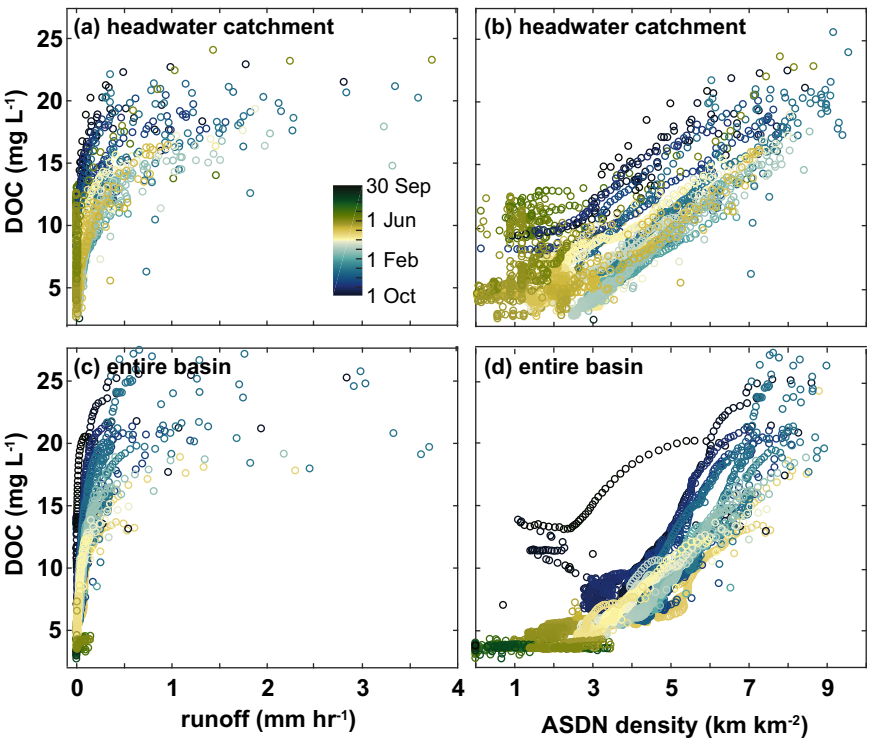

Figure 9. Dissolved organic carbon (DOC) concentrations versus (a) headwater catchment runoff, (b) headwater catchment drainage density, (c) entire basin runoff, and (d) entire basin drainage density. Color gradient represents time.

concentrations displayed a rapid rise from ~1 to 16 mg/L at low to intermediate runoff values (0–0.5 mm/h; Figure 9c). There was strong seasonality in the slope of DOC concentration increases; concentration increases were highest during fall periods and lowest in late spring. Concentrations in summer were always lower. At runoff above 0.5 mm/h, the DOC concentrations plateaued rapidly with seasonally variable DOC concentration maximums. Since ASDN density was calculated as a function of runoff, seasonal patterns between DOC concentrations and ASDN densities were similar to those between DOC concentrations and runoff, although the overall shape of the relationships were different. Low ASDN densities and DOC concentrations were associated with summer and early fall periods, when DOC-limited baseflow sources dominated the runoff signal (Figure 9d). At ASDN densities above approximately 3 km/km^2, a linear increase in DOC concentrations with increasing runoff occurred, with variability driven by season. At very high ASDN densities (>7 km/km^2), the rate of increase in DOC concentrations appeared to begin to flatten.

One precipitation event in early October produced higher DOC concentrations for the observed runoff magnitude than other events with the same runoff (dark blue circles extending from data cloud in Figure 9d). While this unusual event response was clearest at the outlet of the entire basin, it also produced DOC concentrations at the upper range of observed concentrations in the headwater catchment (Figure 9b). This event was one of the first large precipitation events of the water year and was large enough to initiate runoff at the outlet to the entire basin that persisted for the entire fall, winter, and spring seasons (Figure 2c). This large event occurred after several dry months and therefore mobilized a substantial amount of DOC into the stream network (Figure 9). The total DOC flux for this fall event was 3.8 kg/ha, which comprised ~18% of the measured load over the study period (approximately 1 year) at the entire basin outlet.

The DOC fluxes from the headwaters and lowlands showed strong seasonality (Figure 10). The DOC fluxes were greatest during precipitation events in fall, winter, and spring. Lowlands contributed more DOC than headwaters to the entire basin in fall, both during precipitation events and interstorm periods. In early winter periods, the headwaters had higher DOC fluxes than lowlands during precipitation events. During the transition to spring, the headwaters and lowlands had similar DOC fluxes during precipitation events, as well as between events. There were short periods where negative fluxes occurred in the lowlands, which

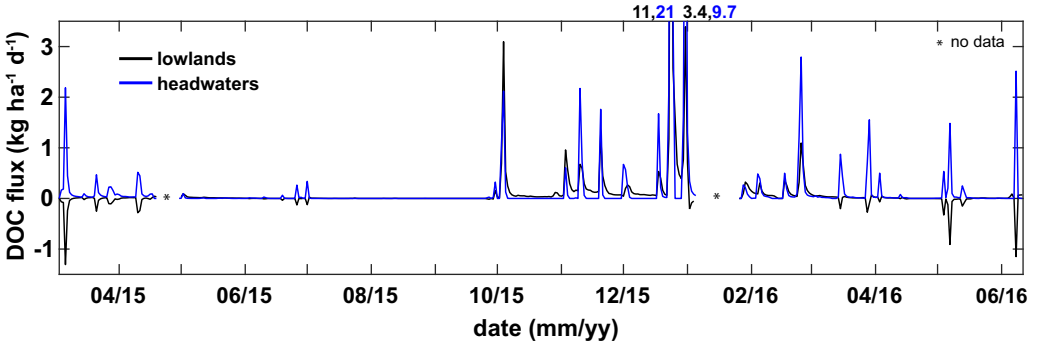

Figure 10. Dissolved organic carbon (DOC) flux (kg/ha/d) from headwaters (blue line) and from lowlands (black line). Small numbers represent peaks above 3.4 kg/ha/d. Asterisks marks periods with missing data. Negative flux values refer to a loss/retention of DOC in the specific landscape element; positive flux values refer to a gain of DOC.

mostly happened in the spring and summer (Figure 10). These negative fluxes may have resulted from differences in transport timing, uptake, adsorption, and/or storage in the lowland system, or from errors from the extrapolation of headwater fluxes from a single gauge.

3.5. Intensively Sampled Precipitation Events With Contrasting Catchment Wetness Conditions

Two intensively sampled precipitation events with contrasting catchment storage states are described in detail in the next two sections as specific examples of the overall hydrochemical dynamics observed at this study site.

3.5.1. Event 1: High Catchment Storage State

Event 1 occurred when catchment storage was high (4–9 March 2015), groundwater levels were elevated, and preevent baseflow was present at the outlets to both the headwater catchment and the entire basin (Figures 11a–11d and 12a–12c). Twenty millimeters of precipitation fell, which produced a runoff ratio of 0.74 at the 3.3 ha headwater catchment outlet and 0.33 at the entire 48.4 ha basin outlet. This event was representative of the general characteristics of events during high catchment storage periods when evapotranspirative demands were low (Table 2), which generally occurred in winter and spring periods (Figure 2). In these periods, runoff ratios were high (Figures 2 and 6) and groundwater from shallow and deep subsurface zones contributed to runoff (Figure 8).

In the headwater catchment, groundwater levels and runoff responded to precipitation simultaneously (Figures 11a–11d). Stream water DOC concentrations increased with increases in runoff, while specific conductance showed a dilution response (Figure 11b). Stream water DOC concentrations were similar in magnitude to concentrations measured in the lower and upper hillslope shallow wells (Figures 11b–11d). The deeper groundwater well in the lower hillslope zone showed a slight increase in DOC concentrations during the event, while the shallow well showed a slight decrease. Concentrations across the variable depth wells converged during the falling limb of the stream hydrograph (Figure 11c). Shallow and deep groundwater in the upper hillslope zone showed similar patterns with an initial increase and then decrease in DOC concentrations, but absolute concentrations were different (Figure 11d).

Runoff at the outlet of the entire basin and groundwater in the lowlands showed similar dynamics to the headwater system in that groundwater and runoff responses to precipitation were simultaneous (Figures 12a–12c). In the stream, DOC concentrations also increased with increases in runoff, while specific conductance showed a dilution response (Figure 12b). Stream water DOC concentrations were similar in magnitude to concentrations measured in the lowlands well (Figure 12c). The DOC concentrations in the groundwater well did not fluctuate substantially (~20 mg/L) and groundwater levels were in the upper 25 cm preevent and reached the ground surface during the event.

3.5.2. Event 2: Low Catchment Storage State

Event 2 occurred when catchment storage was low (2–7 October 2015) and groundwater wells were generally dry. Preevent baseflow was present at the outlet of the entire basin, but the headwater streams were dry (Figures 11e–11h and 12d–12f). Eighty-seven millimeters of precipitation fell, which produced a runoff

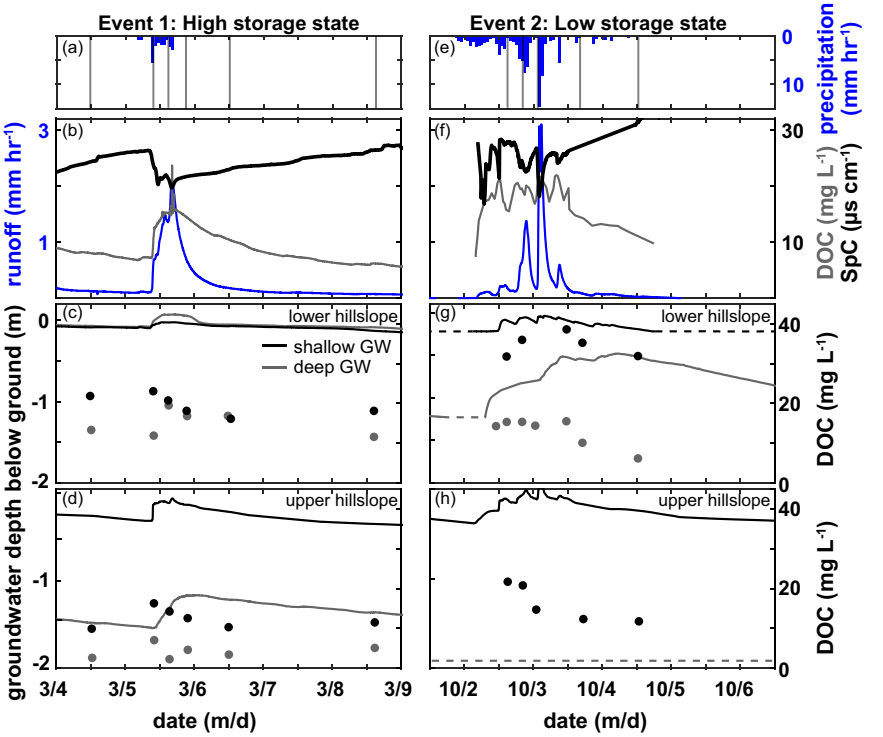

Figure 11. Headwater catchment responses to Event 1 (left column) and Event 2 (right column). Specifically, (a, e) precipitation (blue bars) and sampling times of source and stream waters (grey vertical lines), (b, f) runoff (blue line), DOC (grey line) concentrations, and specific conductance (SpC; black line) at the headwater catchment outlet, (c–d, g–h) shallow (black lines) and deep (grey lines) groundwater water levels and DOC concentrations (black grey circles) in lower hillslope and upper hillslope positions, respectively. Dashed lines represent no groundwater recorded in well (dry).

ratio of 0.18 at both the headwater catchment and entire basin outlets. Runoff responses to this event were characteristic of events during low catchment storage periods when seasonal evapotranspirative demands were high (Table 2), which generally occurred in summer and fall periods (Figure 2). In these periods, runoff

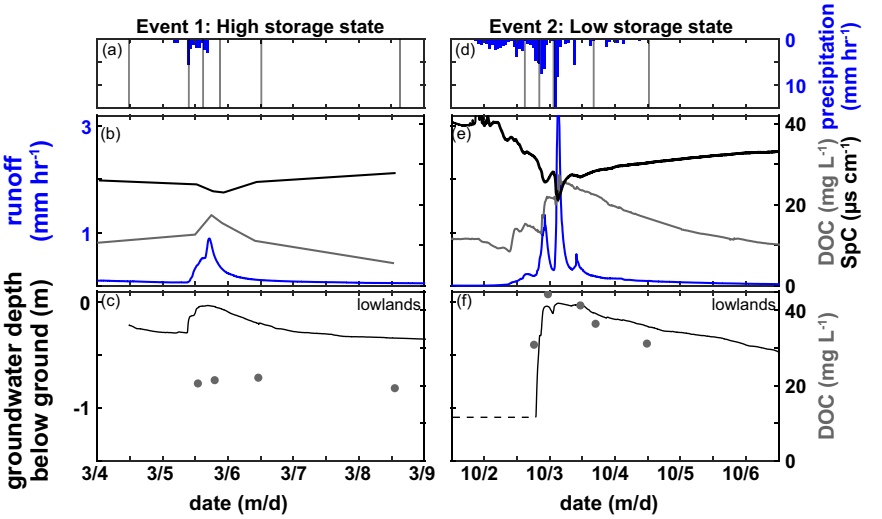

Figure 12. Entire basin outlet responses to Event 1 (left column) and Event 2 (right column). Specifically, (a, d) precipitation (blue bars) and sampling times of source and stream waters (grey vertical lines), (b, e) runoff (blue lines), DOC concentrations (grey lines), and specific conductance (SpC; black lines) at the entire basin outlet, (c, f) groundwater DOC (grey circles) and levels (grey line) in lowlands well. Dashed lines represent no groundwater recorded in well (dry).

ratios were low (Figures 2 and 6) and groundwater contributions from deep subsurface zones were generally not active (Figure 8).

In the headwater catchment, groundwater levels and runoff responses to precipitation were not simultaneous (Figures 11e–11h). Runoff in the channel occurred before any of the deep groundwater wells displayed a hydrologic response but was simultaneous with perched water table responses in the shallow wells in both the upper and lower hillslope (Figures 11g and 11h). In the upper hillslope zone, the deep groundwater well never showed a hydrologic response during this event. In the lower hillslope zone, deep groundwater wells responded after the shallow wells (Figure 11g). Stream DOC concentrations increased rapidly from 7 mg/L at initial runoff activation to a relatively constant concentration of ~20 mg/L throughout the event (Figure 11f). Specific conductance showed a dilution response that mirrored DOC dynamics (Figure 11f). Stream water DOC concentrations were between the high concentrations in the shallow groundwater system and low concentrations in the deep groundwater system in the lower hillslope (Figure 11g). The deeper groundwater well in the lower hillslope zone had stable DOC concentrations during the event and decreasing concentrations during the falling limb (Figure 11g). The shallow well had DOC concentration patterns that mirrored the stream (Figure 11g). The DOC concentrations in the shallow groundwater in the upper hillslope zone decreased at the storm peak (Figure 11h).

Preevent baseflow at the entire basin outlet had low DOC concentrations and high specific conductance (Figure 12e). Groundwater level in the lowlands was below the groundwater well installation/refusal depth (Figure 12f), which coincided with the elevation of the nearby streambed. The stream responded to precipitation roughly 6 h before the groundwater well in the lowlands showed a hydrologic response. When the groundwater did respond, it responded rapidly and water levels reached the ground surface in 3.5 h and stayed at or near the ground surface for the remainder of the event (Figure 12f). Stream water DOC concentrations increased with increases in runoff, while specific conductance showed a dilution response (Figure 12b). The DOC concentrations in the lowlands groundwater well showed a similar temporal pattern. During the event, lowlands groundwater DOC concentrations peaked at 48 mg/L and stream water DOC peaked at 28 mg/L.

4. Discussion

4.1. Longitudinal Network Dynamics as the Surficial Expression of Lateral and Vertical Source Areas Driven by Subsurface Stratigraphy and Evapotranspirative Demands

The location of surface water in geomorphic channel networks can provide valuable information about spatial water availability in the landscape (Godsey & Kirchner, 2014; Whiting & Godsey, 2016; Winter et al., 1998). The climatic and internal catchment thresholds and mechanisms that lead to activation and contraction of longitudinal stream sections across the drainage network are less understood. Here we link longitudinal ASDN dynamics to a process-based understanding of vertical and lateral hydrologic connectivity within the catchment.

4.1.1. Landscape Element Contributions Aggregate to Produce Distinct Basin Outlet Runoff Signals

A comparison of runoff contributions from lowlands and headwaters indicated that runoff contributions across the study site varied through time (Figure 7). During periods of high catchment storage, specifically winter to spring when baseflow was present across the drainage network, the lowlands contributed more runoff to the entire basin than the headwaters, when accounting for areal differences (Figure 7). During precipitation events, especially in late spring through fall when baseflow was low or absent, headwaters contributed more to runoff at the entire basin scale. These headwater-driven event dynamics could be explained by stream water loss (from runoff that originated in the headwaters) to the shallow groundwater system or deeper alluvial aquifer in the lowlands, or to smaller overall runoff contributions from the lowlands, or some combination of both.

The fluctuations in relative runoff contributions from headwaters and lowlands were reflected in event to annual scale runoff ratios (Figure 6). The annual runoff ratio for the water year 2016 was higher in the 3.3 ha headwater catchment (0.39) than at the scale of the entire 48.4 ha basin (0.29; Table 3). With the assumption of spatially uniform evapotranspiration, the annual groundwater recharge ratio was higher at the scale of the entire basin (0.19) than at the scale of the headwater catchment (0.08; Table 3). Together, this suggests that stormflow-driven hydrologic connectivity drove headwater runoff dynamics and longitudinal

connections across the drainage network. These flashy, often perched, stormflow-driven connections resulted in extensive vertical groundwater recharge at the scale of the entire basin. Although the lowlands contributed significant runoff on a seasonal basis, headwaters yielded substantially more runoff during individual precipitation events, especially when the catchment storage state was low (Figures 6 and 7).

4.1.2. Vertically Partitioned Subsurface Flow Paths Drive Landscape Element Runoff Contributions and Drainage Network Dynamics

Due to complex subsurface stratigraphy and structure in watersheds, many streams are fed by nested groundwater systems that can temporarily connect and disconnect vertically due to fluctuations in internal catchment storage and degree of saturation (Kim et al., 2017; Ocampo et al., 2006). In humid Piedmont regions that are typically energy-limited environments, seasonal evapotranspiration can drive catchment storage dynamics across a relatively uniform monthly precipitation regime (Nippgen et al., 2016). This seasonal evapotranspiration regime has been shown to mediate the relative role of deep and shallow groundwater in runoff production in these headwaters (Table 2). Zimmer and McGlynn (2017b) showed that high evapotranspiration rates in summer caused the deep groundwater system to drop below the elevation of the geomorphic channel network in the headwater system. During this time, runoff in headwaters was ephemeral (Figure 2b). While informative, this previous research did not include consideration of the downstream perennial stream network.

Zimmer and McGlynn (2017b) showed that contributions to ephemeral runoff in the headwaters were predominantly generated from precipitation inputs activating the shallow, but not deep, groundwater system (Figures 8a and 8b). This was further highlighted in the headwater catchment groundwater wells in Event 2 (Figure 11). Impeding soil horizons due to shifts in permeability or saturated hydraulic conductivity with depth have been shown to drive the redistribution of water across hillslopes (Elsenbeer, 2001; Heller & Kleber, 2016; McDaniel et al., 2008). These impeding layers can direct rapid subsurface flow paths laterally, while slower vertical percolation through both the soil matrix and preferential pathways can allow a deeper groundwater system to develop simultaneously (Du et al., 2016). In this study, we observed that shallow flow paths dominated runoff dynamics, suggesting an impeding layer strongly routed shallow flow laterally. We showed that stormflow-driven contributions, which were controlled by shallow flow paths, dominated the ASDN expansion in headwaters (Figure 5). Baseflow-associated ASDN expansion comprised a smaller component of drainage network dynamics in the headwaters. The seasonal rise and fall of the deep water table drove this baseflow-associated expansion and contraction during periods of intermittent runoff (Figure 5). As highlighted in the headwater catchment groundwater wells in Event 1 (Figure 11), groundwater levels were elevated prior to the event, which allowed for rapid activation of shallow flow paths during events. This dynamic allowed stormflow-driven ASDN expansion to still play a substantial role during periods of persistent baseflow contributions.

The composition of baseflow-associated versus stormflow-driven ASDN varied across the two watershed scales. The overall influence of baseflow-associated flow paths on network length increased with increasing watershed scale (Figure 5). However, even at the scale of the entire basin, stormflow-driven flow path contributions played an important role in runoff generation and ASDN expansion. The groundwater dynamics in wells located in the lowlands suggested a strong relationship between groundwater levels and runoff regardless of season (Figure 8c). High runoff at the entire basin outlet was dependent on high groundwater levels in the lowlands. However, it is in these landscape positions where the stratigraphy of the subsurface appeared to matter less for runoff generation because the continual rise of the deep water table disallowed any perching of a shallow water table to occur. We observed that lowland groundwater levels flattened out at lower runoff values and at a higher level than the shallow hillslope wells. However, the overall shape of the relationship between lowland groundwater levels and runoff at the entire basin outlet (Figure 8c) was generally similar to the relationship between the shallow, perched, transient water table and runoff in the headwater catchment (Figure 8a). This suggests similar influences of shallow groundwater on runoff across watershed scales. In both Event 1 and 2, lowland groundwater responded to precipitation inputs similarly to shallow groundwater in the headwaters (Figures 11 and 12).

The bedrock groundwater system exhibited strong seasonality that was related to the longitudinal expansion of the baseflow-associated ASDN. The groundwater level rise in the bedrock well was driven by recharge from precipitation, although the amount of percolation was influenced by evapotranspirative demands in the shallower subsurface environment (Figure 8d). When evapotranspiration was low and

shallow soil water content was high, more percolation occurred, which raised the bedrock groundwater levels. When evapotranspiration was high, drainage of the aquifer outpaced vertical recharge. This recharge dynamic mirrored the deep groundwater well in the upper hillslope in the headwater catchment (Figure 8b), suggesting these groundwater systems were vertically connected or representative of the same deep groundwater system. Furthermore, groundwater in these two deep wells showed similar influences on runoff at both watershed scales. Event-driven runoff at the headwater catchment or the entire basin outlet was not related to groundwater dynamics in these deep zones (Figures 8b, 8d, and 11). However, these deep groundwater systems contributed to the spatial presence of baseflow, which was seen in Event 1 when the deep groundwater system was actively contributing to baseflow preevent (Figure 11).

4.2. Lateral, Vertical, and Longitudinal Hydrologic Connectivity Contribute to Seasonal and Event Flushing of Carbon Across Watershed Scales

Across both spatial scales, in-stream DOC concentrations increased in response to increases in runoff (Figures 9a and 9c). This has been seen in a wide range of landscape types, such as boreal landscapes (Laudon et al., 2011), wetlands (Raymond & Hopkinson, 2003), temperate forested landscapes (McGlynn & McDonnell, 2003b; Raymond & Saiers, 2010), and semiarid mountainous regions (Pacific et al., 2010). This is often attributed to lateral or vertical hydrologic connectivity of DOC-rich source areas during periods of runoff activation, such as precipitation events or snowmelt pulses (e.g., Brown et al., 1999; Hornberger et al., 1994). At this study site, we observed a strong influence of shallow subsurface flow paths on runoff magnitudes across both the headwaters and lowlands (Figures 8a and 8c). We also observed high DOC concentrations in groundwater in shallow soils across these landscape elements (Figures 11 and 12). Together, this suggests that both in-stream DOC concentrations and runoff magnitudes were driven predominantly by contributions from shallow subsurface flow paths across this study site.

Many studies attribute the majority of annual DOC export to large, hydrologic events, such as snowmelt (Bass et al., 2011; Botter et al., 2013; Pacific et al., 2010; Pellerin et al., 2012). These large events, particularly when antecedent conditions are wet, flush substantial amounts of DOC from shallow soil horizons. In this study, one large tropical storm occurred during the study period, resulting in a DOC-runoff anomaly (dark blue circles in Figure 9d). This single event accounted for $\sim$18% of the DOC flux recorded in $\sim$1 year. Barring such anomalous precipitation amounts from hurricanes or tropical storms, monthly precipitation in this Piedmont landscape is relatively uniform (Figure 2). As a result, we observed continual and substantial flushing of DOC from shallow soil horizons during most precipitation events (Figures 11 and 12). This produced high DOC fluxes and concentrations during precipitation events year round (Figures 9 and 10).

Researchers have shown that repeated flushing of shallow soils can result in depleted pools of DOC through seasons (Boyer et al., 1997; Lambert et al., 2014). At this site, there was seasonal variability in the in-stream DOC concentrations-runoff relationships (Figure 9). This seasonal variation occurred across both watershed scales and was most apparent at high runoff (Figures 9a and 9c). In-stream DOC concentrations decreased throughout the water year; events in fall and early winter were associated with the highest DOC concentrations and events in late spring and summer had the lowest DOC concentrations (Figures 9a and 9c). The decrease in stream water DOC concentrations in late spring and summer was unlikely due to deeper groundwater contributions because groundwater levels were low or absent during these times (Figures 8b and 8d). Other studies have shown that DOC source depletion can occur due to frequent flushing of shallow subsurface soils across subsequent precipitation events through the year (Boyer et al., 1997) and this likely explains the observed seasonal differences in DOC concentrations here as well.

Landscape element composition, terrain characteristics, and hydrologic processes in watersheds have been shown to drive DOC responses to precipitation inputs (Creed & Band, 1998; Inamdar & Mitchell, 2006; McGlynn & McDonnell, 2003a; Pacific et al., 2010). This study site was composed of two dominant landscape elements. The headwaters were composed of steeper slopes and deeper soils, while the downstream lowlands were composed of gentler slopes and shallower soils (Figure 1). With increasing watershed size, the relative spatial extent of these two systems shifted from predominantly headwaters to lowlands. In-stream DOC concentrations across watershed scales reflected distinct hydrologic and biogeochemical influences associated with this topographic and landscape element composition shift (Figures 9b and 9d). In the 3.3 ha headwater catchment, stream water DOC concentrations were influenced by season, especially in low flow periods. For instance, given similar runoff and longitudinal network lengths, in-stream DOC

concentrations were higher in late summer than late spring (Figure 9b). At the 48.4 ha basin outlet, in-stream DOC showed much less spread in possible concentrations with a given runoff magnitude. This difference across spatial scales was most likely driven by the composition of source areas that mediate the ASDN at lower flows. In the headwaters, summertime network dynamics were driven entirely by shallow surface and subsurface stormflow, with variable concentrations of DOC, dependent on availability of DOC in the shallow flow paths (Brown et al., 1999; Futter et al., 2007). In the lowlands, baseflow was present during much of the summer. Baseflow contributions from deeper groundwater supported the majority of ASDN length at low flows ($<\sim$3 km/km^2). These deeper groundwater sources typically have a lower DOC concentration than shallower stormflow-activated subsurface sources (Figures 11c, 11d, 11g, and 11h) and thus reduced DOC concentration variability at low flows and ASDN densities at the basin outlet (Figures 9c and 9d). Stormflow-activated shallow flow paths led to the rapid increase in DOC concentrations seen at ASDN densities $>\sim$3 km/km^2.

4.3. Intensively Sampled Precipitation Events Demonstrate Characteristic Event Dynamics Across Catchment Storage States

Recent studies that have explored ASDN dynamics either do so through seasonal "snapshots" of the active network (Godsey & Kirchner, 2014; Jensen et al., 2017; Shaw, 2016; Whiting & Godsey, 2016; Zimmer et al., 2013) or through model investigations that do not include field observations (Biswal & Marani, 2010). While "snapshots" can provide valuable information on network extents at selected wetness states, the dynamic behavior arising from spatiotemporally complex runoff generation processes at intra-seasonal time scales can be missed. For this study, we paired detailed observations of source area dynamics during two events with longer term, continuous hydrochemical, runoff, and ASDN data. Here we link these results to the overall dynamics seen seasonally across the two watershed scales to provide a more mechanistic understanding of ASDN expansion and contraction and its influence on observed biogeochemical patterns.

During events with high antecedent wetness, the headwater and entire basin runoff ratios showed proportional increases at high runoff ratios (Figure 6). Event 1 was a precipitation event that occurred when catchment storage was high and thus can be used to better understand overarching processes that drive these spatial runoff relationships. Groundwater levels were elevated prior to the event and baseflow-associated ASDN connectivity between the headwaters and downstream lowlands was already present. Precipitation inputs produced an expansion of source areas across the catchment from the rise of deeper groundwater into shallow soil horizons within both the headwaters and lowlands. In the headwaters, in-stream DOC concentrations peaked with runoff (Figure 11b). With fewer samples collected from the entire basin outlet, it is unclear how the timing of in-stream DOC concentrations paired with runoff, but similar behavior is apparent across the two watershed scales (Figure 12b). Groundwater DOC concentrations were relatively similar laterally along hillslopes, vertically with depth, and spatially across watershed scales (Figures 11c and 11d). The dominant spatial runoff and DOC contributors across the study site thus appeared to be relatively homogeneous, highly connected, and rich in DOC. Together, these dynamics mechanistically explained the proportional increases in runoff ratios and consistent DOC concentrations across watershed scales during high antecedent storage events.

For low catchment storage state events, runoff ratios were higher in the 3.3 ha headwater catchment than at the scale of the entire 48.4 ha basin (Figure 6). This suggests runoff generation across the study site was not homogeneous at low storage states. Event runoff magnitudes did not statistically explained the ratio of runoff ratios (Table 4). In contrast, the event runoff magnitudes at each individual scale explained a significant amount of variability in the runoff ratios (Table 4). This suggests that the processes that produced runoff in the headwaters do not simply scale up to explain the runoff dynamics observed at the entire basin outlet.

An example of these spatially diverse runoff generation processes can be seen in Event 2, when catchment storage and groundwater levels were low (most wells were dry) prior to the event (Figures 11 and 12). Precipitation inputs drove activation of different source areas depending on location. In the headwaters, precipitation inputs activated only shallow, perched, transient water tables. These shallow flow paths contributed substantial DOC and water to the stream. In the lowlands, precipitation inputs activated the deeper water table, which rose up into shallow soil horizons. These different processes led to changes in the ASDN that resulted in distinct in-stream DOC signals across watershed scales (Figures 11f and 12e). In

the headwaters, immediate activation of shallow flow paths resulted in stream DOC concentration that rose rapidly and stayed relatively consistent throughout Event 2. At the scale of the entire basin, in-stream DOC concentrations increased throughout the event. This downstream response may be an expression of increasing hydrologic connections between the basin outlet and distal, DOC-rich landscape positions. Together, these DOC dynamics reflect the different mechanisms that lead to distinct hydrochemical behavior across watershed scales.

4.4. Linking Longitudinal Stream Network Expansion and Lateral and Vertical Source Area Connectivity to Explain Hydrobiogeochemical Signals Across Watershed Scales

Lateral contributions from hillslopes or landscape units have been suggested to drive runoff generation and in-stream chemistry (Jencso & McGlynn, 2011; McGlynn & McDonnell, 2003b; Tetzlaff et al., 2015; van Meerveld et al., 2015; van Verseveld et al., 2008). As watershed scale increases, upstream contributions (e.g., from longitudinal ASDN connectivity) can play a more significant role in hydrochemistry (Webster, 2007). The longitudinal expansion of the ASDN can provide hydrologic connection between the stream and distal portions of the landscape, shaping stream chemistry signatures. Despite this, the linkages between longitudinal network activation, spatially complex runoff mechanisms, and hydrochemistry at the watershed outlet are still unclear. In this study, we linked observations of geomorphically partitioned deep and shallow groundwater contributions, ASDN expansion and contraction, and water and DOC export across two watershed scales, in an effort to address some of these knowledge gaps.

Here we present a multidimensional source area activation conceptual framework to explain runoff and chemistry across the drainage network that builds on the plethora of previous catchment hydrology. From observations of precipitation, runoff, and dominant runoff-generating flow paths, we demonstrated two dominant processes that drove ASDN expansion and contraction across two watershed scales. Baseflow-associated flow paths comprised the seasonal expansion and contraction of the active surface drainage network. These flow paths were dominated by deeper groundwater sources that were strongly influenced by evapotranspirative demands and climatic forcings characteristic of the humid, subtropical climate of the Piedmont. Stormflow-driven flow paths led to the event-based expansion and contraction of the drainage network. These flow paths were activated by both shallow and deep groundwater sources, dependent on catchment storage and critical zone architecture (e.g., subsurface structure and stratigraphy) across the landscape.

This differential source area activation drove event and seasonal dynamics in stream water DOC concentrations. While in-stream DOC concentrations consistently increased with increases in runoff across individual events and seasons, the variability in DOC concentrations across specific runoff magnitudes shifted (Figure 9). As shallow flow paths were activated during stormflow-driven network expansion, DOC was mobilized frequently from shallow soil horizons (Figure 9) as well as spatially across both headwater and lowland landscape elements (Figure 10). This frequent DOC flushing resulted in source depletion on an annual basis. In fall, in-stream DOC concentrations were high due to shallow flow path interactions with, and mobilization of, fresh litterfall. By spring and summer, in-stream DOC concentrations were lower given similar runoff magnitudes, due to source depletion. This seasonal and event-driven DOC-runoff relationship was observed at the scale of the headwaters, as well as the scale of the entire basin, which encompassed both headwaters and lowlands. Dilution of these shallow DOC-rich flow paths may also occur as storage state increases due to increased connection to deep groundwater contributions (Figure 8). This mechanism, however, would not explain a decrease in stream water DOC concentrations in summer in the headwater catchment where contributions from deep groundwater were minimal or absent (Figure 8b). From these observed ASDN and DOC seasonal and event dynamics, we suggest that the hydrological and chemical signals at larger watershed outlets can be driven by a balance of lateral, longitudinal, and vertical source areas, flow pathways, and hydrologic processes internal to the basin. Continual work encompassing multidimensional source area dynamics may further help elucidate complex hydrobiogeochemical dynamics seen at watershed outlets in other landscapes and climates.

5. Conclusions

We used a data-driven approach to develop a seasonal and event-based conceptual model of vertical and lateral flow path contributions to active surface drainage network (ASDN) expansion and DOC export across an ephemeral-to-perennial drainage network composed of headwater and lowland landscape elements. We

characterized the timing and magnitude of precipitation, runoff, and the dominant runoff-generating flow paths across these landscape elements to (1) decipher the internal catchment processes that drive the activation of runoff across watershed scales and (2) investigate how this differential activation of runoff can impact surface drainage and biogeochemical dynamics at the larger basin outlet.

Our results suggest that the vertical partitioning of shallow and deep groundwater contributions to runoff produced an ASDN that was composed of two superimposed runoff regimes. We showed that portions of the ASDN were composed of baseflow-associated and stormflow-driven flow paths that fluctuated in spatial extent seasonally and episodically. Deeper baseflow-associated flow paths dominated much of the ASDN across the lowlands, while shallow stormflow-driven flow paths dominated much of the ASDN in the headwaters. Together, these differential source areas drove DOC export dynamics. The presence of shallow stormflow-driven flow paths across headwaters and lowlands drove an increase in stream water DOC concentrations with increases in runoff. Within this DOC-runoff relationship, seasonal variability in stream water DOC concentrations showed a depletion of carbon stores in shallow soil zones due to flushing from frequent shallow subsurface flow path activation or dilution from the connection with DOC-poor deeper groundwater. Therefore, observed in-stream DOC dynamics were a manifestation of shifting runoff sources, runoff-generating flow paths, and depleted DOC availability in space and time. Future research could include quantifying runoff and DOC contributions from different dimensional source areas.

The conceptual model we presented in this study spanned both ephemeral and intermittent headwater catchments and their downstream perennial waterways to explain how hydrobiogeochemical signals at larger watershed outlets can be driven by a balance of hydrologic contributions from lateral, longitudinal, and vertical source area connectivity, as well as event-driven flushing that leads to seasonal solute depletion. Although focused on the Piedmont landscape of North Carolina, USA, we suggest that this work is widely relevant in systems, specifically low relief, where deep and shallow runoff generation processes occur and the ASDN expands and contracts seasonally as well as in response to precipitation or snowmelt inputs.

Acknowledgments
This study was made possible by a National Science Foundation Graduate Research Fellowship to M.A. Zimmer, Duke University funding to B.L. McGlynn, and funding through the Calhoun Critical Zone Observatory. The authors thank Stephen Architzel, Cassandra Harvey, Harley Burton, Mary Tchamkina, and Ethan Blatt for extensive field and lab work assistance and to Daniel Richter for collaboration and site access to the Duke Forest Research Watershed, a satellite site to the Calhoun Critical Zone Observatory. Historical evapotranspiration data can be downloaded at http://ameriflux.lbl.gov. All other hydrometric data is discoverable in the CUAHSI Hydroshare data repository at https://www.hydroshare.org. Finally, we thank Genevieve Ali, the Associate Editor, Ilja van Meerveld, and two anonymous reviewers for comments on early versions, which greatly improved our manuscript.

References

Ågren, A., Buffam, I., Jansson, M., & Laudon, H. (2007). Importance of seasonality and small streams for the landscape regulation of dissolved organic carbon export. *Journal of Geophysical Research*, *112*, G03003. https://doi.org/10.1029/2006JG000381

Allan, C. J., & Roulet, N. T. (1994). Runoff generation in zero-order precambrian shield catchments—The stormflow response of a heterogeneous landscape. *Hydrological Processes*, *8*(4), 369–388. https://doi.org/10.1002/hyp.3360080409

Allen, G. H., Pavelsky, T. M., Barefoot, E. A., Lamb, M. P., Butman, D., Tashie, A. M., et al. (2018). Similarity of stream width distributions across headwater systems. *Nature Communications*, *9*, 610. https://doi.org/10.1038/s41467-018-02991-w

Bass, A. M., Bird, M. I., Liddell, M. J., & Nelson, P. N. (2011). Fluvial dynamics of dissolved and particulate organic carbon during periodic discharge events in a steep tropical rainforest catchment. *Limnology and Oceanography*, *56*(6), 2282–2292. https://doi.org/10.4319/lo.2011.56.6.2282

Bishop, K. H., Lundström, U. S., & Giesler, R. (1993). Transfer of organic C from forest soils to surface waters: Example from northern Sweden. *Applied Geochemistry*, *8*(2), 11–15. https://doi.org/10.1016/S0883-2927(09)80003-6

Biswal, B., & Marani, M. (2010). Geomorphological origin of recession curves. *Geophysical Research Letters*, *37*, L24403. https://doi.org/10.1029/2010GL045415

Blyth, K., & Rodda, J. C. (1973). A stream length study. *Water Resources Research*, *9*(5), 1454–1461. https://doi.org/10.1029/WR009i005p01454

Botter, G., Basso, S., Rodriguez-Iturbe, I., & Rinaldo, A. (2013). Resilience of river flow regimes. *Proceedings of the National Academy of Sciences of the United States of America*, *110*(32), 12925–12930. https://doi.org/10.1073/pnas.1311920110

Boyer, E. W., Hornberger, G. M., Bencala, K. E., & McKnight, D. M. (1997). Response characteristics of DOC flushing in an alpine catchment. *Hydrological Processes*, *11*(12), 1635–1647. https://doi.org/10.1002/(SICI)1099-1085(19971015)11:12<1635::AID-HYP494>3.0.CO;2-H

Bracken, L. J., Wainwright, J., Ali, G. A., Tetzlaff, D., Smith, M. W., Reaney, S. M., et al. (2013). Concepts of hydrological connectivity: Research approaches, Pathways and future agendas. *Earth-Science Reviews*, *119*, 17–34. https://doi.org/10.1016/j.earscirev.2013.02.001

Bradley, P. J., & Gay, N. K. (2005). *Geologic map of Hillsborough 7.5-minute quadrangle, Orange County, North Carolina* (Open File Rep. 2005 02, scale 1:24,000, in color). North Carolina Geological Survey.

Brown, V. A., McDonnell, J. J., Burns, D. A., & Kendall, C. (1999). The role of event water, a rapid shallow flow component, and catchment size in summer stormflow. *Journal of Hydrology*, *217*(3–4), 171–190. https://doi.org/10.1016/S0022-1694(98)00247-9

Budyko, M. I. (1974). *Climate and life*. Cambridge, MA: Academic.

Covino, T. (2017). Hydrologic connectivity as a framework for understanding biogeochemical flux through watersheds and along fluvial networks. *Geomorphology*, *277*, 133–144. https://doi.org/10.1016/j.geomorph.2016.09.030

Covino, T. P., & McGlynn, B. L. (2007). Stream gains and losses across a mountain-to-valley transition: Impacts on watershed hydrology and stream water chemistry. *Water Resources Research*, *43*, W10431. https://doi.org/10.1029/2006WR005544

Creed, I. F., & Band, L. E. (1998). Export of nitrogen from catchments within a temperate forest: Evidence for a unifying mechanism regulated by variable source area dynamics. *Water Resources Research*, *34*(11), 3105. https://doi.org/10.1029/98WR01924

Creed, I. F., McKnight, D. M., Pellerin, B. A., Green, M. B., Bergamaschi, B. A., Aiken, G. R., et al. (2015). The river as a chemostat: Fresh perspectives on dissolved organic matter flowing down the river continuum. *Canadian Journal of Fisheries and Aquatic Sciences*, *72*, 1272–1285. https://doi.org/10.1139/cjfas-2014-0400

Day, D. G. (1978). Drainage density and streamflow. *Earth Surface Processes*, *3*, 319–326.

Detty, J. M., & McGuire, K. J. (2010). Threshold changes in storm runoff generation at a till-mantled headwater catchment. *Water Resources Research*, *46*, W07525. https://doi.org/10.1029/2009WR008102

Du, E., Rhett Jackson, C., Klaus, J., McDonnell, J. J., Griffiths, N. A., Williamson, M. F., et al. (2016). Interflow dynamics on a low relief forested hillslope: Lots of fill, little spill. *Journal of Hydrology*, *534*, 648–658. https://doi.org/10.1016/j.jhydrol.2016.01.039

Dunne, T. (1978). Field studies of hillslope flow processes. In M. J. Kirkby (Ed.), *Hlllslope Hydrology* (pp. 227–293). New York, NY: John Wiley.

Elsenbeer, H. (2001). Hydrologic flowpaths in tropical rainforest soilscapes—A review. *Hydrological Processes*, *15*(10), 1751–1759. https://doi.org/10.1002/hyp.237

Futter, M. N., Butterfield, D., Cosby, B. J., Dillon, P. J., Wade, A. J., & Whitehead, P. G. (2007). Modeling the mechanisms that control in-stream dissolved organic carbon dynamics in upland and forested catchments. *Water Resources Research*, *43*, W02424. https://doi.org/10.1029/2006WR004960

Gannon, J. P., Bailey, S. W., McGuire, K. J., & Shanley, J. B. (2015). Flushing of distal hillslopes as an alternative source of stream dissolved organic carbon in a headwater catchment. *Water Resources Research*, *51*, 1–15. https://doi.org/10.1002/2015WR016927

Godsey, S. E., & Kirchner, J. W. (2014). Dynamic, discontinuous stream networks: Hydrologically driven variations in active drainage density, flowing channels, and stream order. *Hydrological Processes*, *28*, 5791–5803. https://doi.org/10.1002/hyp.10310

Heeren, D. M., Fox, G. A., Miller, R. B., Storm, D. E., Fox, A. K., Penn, C. J., et al. (2011). Stage-dependent transient storage of phosphorus in alluvial floodplains. *Hydrological Processes*, *25*(20), 3230–3243. https://doi.org/10.1002/hyp.8054

Heeren, D. M., Fox, G. A., Storm, D. E., & Miller, R. B. (2014). Divergence and flow direction as indicators of subsurface heterogeneity and stage-dependent storage in alluvial floodplains, *Hydrological Processes*, *28*(3), 1307–1317.

Heller, K., & Kleber, A. (2016). Hillslope runoff generation influenced by layered subsurface in a headwater catchment in Ore Mountains, Germany. *Environmental Earth Sciences*, *75*(11), 1–15. https://doi.org/10.1007/s12665-016-5750-y

Hewlett, J. D., & Hibbert, A. R. (1967). Factors affecting the response of small watershed to precipitation in humid areas. *Forest Hydrology*, 275–279. https://doi.org/10.1177/0309133309338118

Hornberger, G. M., Bencala, K. E., & McKnight, D. M. (1994). Hydrological controls on dissolved organic carbon during snowmelt in the Snake River near Montezuma, Colorado. *Biogeochemistry*, *25*(3), 147–165. https://doi.org/10.1007/BF00024390

Inamdar, S., Rupp, J., & Mitchell, M. (2008). Differences in dissolved organic carbon and nitrogen responses to storm-event and groundwater conditions in a forested, glaciated watershed in western New York. *Journal of the American Water Resources Association*, *44*(6), 1458–1473. https://doi.org/10.1111/j.1752-1688.2008.00251.x

Inamdar, S. P., & Mitchell, M. J. (2006). Hydrologic and topographic controls on storm-event exports of dissolved organic carbon (DOC) and nitrate across catchment scales. *Water Resources Research*, *42*, W03421. https://doi.org/10.1029/2005WR004212

Jencso, K. G., & McGlynn, B. L. (2011). Hierarchical controls on runoff generation: Topographically driven hydrologic connectivity, geology, and vegetation. *Water Resources Research*, *47*, W11527. https://doi.org/10.1029/2011WR010666

Jencso, K. G., McGlynn, B. L., Gooseff, M. N., Wondzell, S. M., Bencala, K. E., & Marshall, L. A. (2009). Hydrologic connectivity between landscapes and streams: Transferring reach- and plot-scale understanding to the catchment scale. *Water Resources Research*, *45*, W04428. https://doi.org/10.1029/2008WR007225

Jensen, C. K., McGuire, K. J., & Prince, P. S. (2017). Headwater stream length dynamics across four physiographic provinces of the Appalachian Highlands. *Hydrological Processes*, *31*(19), 3350–3363. https://doi.org/10.1002/hyp.11259

Kalbitz, K., Solinger, S., Park, J. H., Michalzik, B., & Matzner, E. (2000). Controls on the dynamics of dissolved organic matter in soils: A review. *Soil Science*, *165*(4), 277–304.

Kim, H., Dietrich, W. E., Thurnhoffer, B. M., Bishop, J. K. B., & Fung, I. Y. (2017). Controls on solute concentration-discharge relationships revealed by simultaneous hydrochemistry observations of hillslope runoff and stream flow: The importance of critical zone structure. *Water Resources Research*, *53*, 1424–1443. https://doi.org/10.1002/2016WR019722

Lambert, T., Pierson-Wickmann, A. C., Gruau, G., Jaffrezic, A., Petitjean, P., Thibault, J. N., et al. (2014). DOC sources and DOC transport pathways in a small headwater catchment as revealed by carbon isotope fluctuation during storm events. *Biogeosciences*, *11*(11), 3043–3056. https://doi.org/10.5194/bg-11-3043-2014

Laudon, H., Berggren, M., Ågren, A., Buffam, I., Bishop, K., Grabs, T., et al. (2011). Patterns and dynamics of dissolved organic carbon (DOC) in boreal streams: The role of processes, connectivity, and scaling. *Ecosystems*, *14*(6), 880–893. https://doi.org/10.1007/s10021-011-9452-8

McDaniel, P. A., Regan, M. P., Brooks, E., Boll, J., Barndt, S., Falen, A., et al. (2008). Linking fragipans, perched water tables, and catchment-scale hydrological processes. *Catena*, *73*(2), 166–173. https://doi.org/10.1016/j.catena.2007.05.011

McGlynn, B. L., & McDonnell, J. J. (2003a). Quantifying the relative contributions of riparian and hillslope zones to catchment runoff. *Water Resources Research*, *39*(11), 1310. https://doi.org/10.1029/2003WR002091

McGlynn, B. L., & McDonnell, J. J. (2003b). Role of discrete landscape units in controlling catchment dissolved organic carbon dynamics. *Water Resources Research*, *39*(4), 1090. https://doi.org/10.1029/2002WR001525

McGlynn, B. L., McDonnell, J. J., Seibert, J., & Kendall, C. (2004). Scale effects on headwater catchment runoff timing, flow sources, and groundwater-streamflow relations. *Water Resources Research*, *40*, W07504. https://doi.org/10.1029/2003WR002494

McNamara, J. P., Chandler, D., Seyfried, M., & Achet, S. (2005). Soil moisture states, lateral flow, and streamflow generation in a semi-arid, snowmelt-driven catchment. *Hydrological Processes*, *19*(20), 4023–4038. https://doi.org/10.1002/hyp.5869

McNamara, J. P., Tetzlaff, D., Bishop, K., Soulsby, C., Seyfried, M., Peters, N. E., et al. (2011). Storage as a metric of catchment comparison. *Hydrological Processes*, *25*(21), 3364–3371. https://doi.org/10.1002/hyp.8113

Montgomery, D. R., & Dietrich, W. E. (1994). A physically based model for the topographic control on shallow landsliding. *Water Resources Research*, *30*(4), 1153–1171. https://doi.org/10.1029/93WR02979

Nippgen, F., Mcglynn, B. L., & Emanuel, R. E. (2015). The spatial and temporal evolution of contributing areas. *Water Resources Research*, *51*, 4550–4573. https://doi.org/10.1002/2014WR016719

Nippgen, F., Mcglynn, B. L., Emanuel, R. E., & Vose, J. M. (2016). Watershed memory at the Coweeta Hydrologic Laboratory: The effect of past precipitation and storage on hydrologic response. *Water Resources Research*, *52*, 1673–1695. https://doi.org/10.1002/2015WR018196

NOAA. (2017). *NOAA National Centers for Environmental information, Climate at a Glance: U.S. Time Series*. October 2017. Retrieved from http://www.ncdc.noaa.gov/cag/

Novick, K. A., Oishi, A. C., Ward, E. J., Siqueira, M. B. S., Juang, J. Y., et al. (2015). On the difference in the net ecosystem exchange of CO_2 between deciduous and evergreen forests in the southeastern United States. *Global Change Biology*, *21*(2), 827–842. https://doi.org/10.1111/gcb.12723

Ocampo, C. J., Oldham, C. E., Sivapalan, M., & Turner, J. V. (2006). Hydrological versus biogeochemical controls on catchment nitrate export: A test of the flushing mechanism. *Hydrological Processes*, *20*(20), 4269–4286. https://doi.org/10.1002/hyp.6311

Oishi, A. C., Oren, R., & Stoy, P. C. (2008). Estimating components of forest evapotranspiration: A footprint approach for scaling sap flux measurements. *Agricultural and Forest Meteorology*, *148*, 1719–1732. https://doi.org/10.1016/j.agrformet.2008.06.013

Pacific, V. J., Jencso, K. G., & McGlynn, B. L. (2010). Variable flushing mechanisms and landscape structure control stream DOC export during snowmelt in a set of nested catchments. *Biogeochemistry*, *99*(1), 193–211. https://doi.org/10.1007/s10533-009-9401-1

Pellerin, B. A., Saraceno, J. F., Shanley, J. B., Sebestyen, S. D., Aiken, G. R., Wollheim, W. M., et al. (2012). Taking the pulse of snowmelt: In situ sensors reveal seasonal, event and diurnal patterns of nitrate and dissolved organic matter variability in an upland forest stream. *Biogeochemistry*, *108*(1–3), 183–198. https://doi.org/10.1007/s10533-011-9589-8

Phillips, R. W., Spence, C., & Pomeroy, J. W. (2011). Connectivity and runoff dynamics in heterogeneous basins. *Hydrological Processes*, *25*(19), 3061–3075. https://doi.org/10.1002/hyp.8123

Raymond, P. A., & Hopkinson, C. S. (2003). Ecosystem modulation of dissolved carbon age in a temperate marsh-dominated estuary. *Ecosystems*, *6*(7), 694–705. https://doi.org/10.1007/s10021-002-0213-6

Raymond, P. A., & Saiers, J. E. (2010). Event controlled DOC export from forested watersheds. *Biogeochemistry*, *100*(1), 197–209. https://doi.org/10.1007/s10533-010-9416-7

Richter, D. D., Markewitz, D., Trumbore, S. E., & Wells, C. G. (1999). Rapid accumulation and turnover of soil carbon in a re-establishing forest. *Nature*, *400*(6739), 56–58. https://doi.org/10.1038/21867

Shaw, S. B. (2016). Investigating the linkage between streamflow recession rates and channel network contraction in a mesoscale catchment in New York state. *Hydrological Processes*, *30*(3), 479–492. https://doi.org/10.1002/hyp.10626

Soil Survey Staff. (2016). *Web* soil survey. Nashville, TN: Natural Resources Conservation Service, United States Department of Agriculture. Retrieved from http://websoilsurvey.nrcs.usda.gov/

Spence, C. (2007). On the relation between dynamic storage and runoff: A discussion on thresholds, efficiency, and function. *Water Resources Research*, *43*, W12416. https://doi.org/10.1029/2006WR005645

Tague, C., Grant, G., Farrell, M., Choate, J., & Jefferson, A. (2008). Deep groundwater mediates streamflow response to climate warming in the Oregon Cascades. *Climatic Change*, *86*(1–2), 189–210. https://doi.org/10.1007/s10584-007-9294-8

Temnerud, J., & Bishop, K. (2005). Spatial variation of streamwater chemistry in two Swedish boreal catchments: Implications for environmental assessment. *Environmental Science & Technology*, *39*(6), 1463–1469. https://doi.org/10.1021/es040045q

Tetzlaff, D., Buttle, J., Carey, S. K., Mcguire, K., Laudon, H., & Soulsby, C. (2015). Tracer-based assessment of flow paths, storage and runoff generation in northern catchments: A review. *Hydrological Processes*, *29*(16), 3475–3490. https://doi.org/10.1002/hyp.10412

U.S. Department of Agriculture. (1972). *Field manual for research in agricultural hydrology*. Washington, DC: Author.

van Meerveld, H. J., Seibert, J., & Peters, N. E. (2015). Hillslope-riparian-stream connectivity and flow directions at the Panola Mountain Research Watershed. *Hydrological Processes*, *29*(16), 3556–3574. https://doi.org/10.1002/hyp.10508

van Verseveld, W. J., McDonnell, J. J., & Lajtha, K. (2008). A mechanistic assessment of nutrient flushing at the catchment scale. *Journal of Hydrology*, *358*(3–4), 268–287. https://doi.org/10.1016/j.jhydrol.2008.06.009

Vidon, P. G. F., & Hill, A. R. (2004). Landscape controls on the hydrology of stream riparian zones. *Journal of Hydrology*, *292*(1–4), 210–228. https://doi.org/10.1016/j.jhydrol.2004.01.005

Ward, J. (1989). The four-dimensional nature of lotic ecosystems. *Journal of the North American Benthological Society*, *8*(1), 2–8.

Webster, J. R. (2007). Spiraling down the river continuum: Stream ecology and the U-shaped curve. *Journal of the North American Benthological Society*, *26*(3), 375–389. https://doi.org/10.1899/06-095.1

Whiting, J. A., & Godsey, S. E. (2016). Discontinuous headwater stream networks with stable flowheads, Salmon River basin, Idaho. *Hydrological Processes*, *30*(13), 2305–2316. https://doi.org/10.1002/hyp.10790

Wilson, J. L., & Guan, H. (2004). Mountain-block hydrology and mountain-front recharge. In *Groundwater recharge in a desert environment: The Southwestern United States*. Washington, DC: AGU. https://doi.org/10.1029/009WSA08

Winter, T. C., Harvey, J. W., Franke, O. L., & Alley, W. M. (1998). *Ground water and surface water: A single resource* (Circular 1139). Reston, VA: US Geological Survey.

Wolock, D. M. (2003). *Base-flow index grid for the conterminous United States* (Open File Rep. 03–263). Reston, VA: US Geological Survey.

Wolock, D. M., Fan, J., & Lawrence, G. B. (1997). Effects of basin size on low-flow stream chemistry and subsurface contact time in the Neversink River watershed, New York. *Hydrological Processes*, *11*, 1273–1286. https://doi.org/10.1002/(SICI)1099-1085(199707)11:9<1273::AID-HYP557>3.0.CO;2-S

Zehe, E., Becker, R., Bárdossy, A., & Plate, E. (2005). Uncertainty of simulated catchment runoff response in the presence of threshold processes: Role of initial soil moisture and precipitation. *Journal of Hydrology*, *315*(1–4), 183–202. https://doi.org/10.1016/j.jhydrol.2005.03.038

Zimmer, M. A., Bailey, S. W., Mcguire, K. J., & Bullen, T. D. (2013). Fine scale variations of surface water chemistry in an ephemeral to perennial drainage network. *Hydrological Processes*, *27*(24), 3438–3451. https://doi.org/10.1002/hyp.9449

Zimmer, M. A., & McGlynn, B. L. (2017a). Bidirectional stream–groundwater flow in response to ephemeral and intermittent streamflow and groundwater seasonality. *Hydrological Processes*, *31*, 3871–3880, https://doi.org/10.1002/hyp.11301

Zimmer, M. A., & McGlynn, B. L. (2017b). Ephemeral and intermittent runoff generation processes in a low relief, highly weathered catchment. *Water Resources Research*, *53*, 7055–7077. https://doi.org/10.1002/2016WR019742

Zimmer, M. A., & McGlynn, B. L. (2017c). Time-lapse animation of hillslope groundwater dynamics details event-based and seasonal bidirectional stream–groundwater gradients. *Hydrological Processes*, *31*(10), 1983–1985. https://doi.org/10.1002/hyp.11124